Response to Reviewer 2 (RC2)

Manuscript egusphere-2026-457: "Country-wide rainfall estimates from a commercial microwave link network in Belgium", by K. Van Weverberg et al.

General response

We thank the reviewer for the careful reading of the manuscript and for identifying several inconsistencies and points requiring clarification. All of them have been addressed in the revision. Reviewer comments are reproduced in blue italics, followed by our response and the corresponding changes to the manuscript. Where we quote from the revised manuscript, the text is given in italics between quotation marks. Since a revised manuscript cannot be uploaded during this response phase, we refer to the section, figure and table numbers of the revised manuscript throughout, and we reproduce the relevant new figures and tables at the end of this document.

We note first that the two reviewers' suggestions prompted a substantially deeper revision of the retrieval pipeline than the individual points below might suggest (a more thorough quality assessment of the disdrometers (leading to the removal of one instrument), a more consistent formulation of the attenuation–rain-rate relation fitted directly in the retrieval (R–γ) direction and compared like-for-like with previous studies, and an α-weighting of the minimum and maximum rain rates that accounts for the skewness of sub-window rainfall following Overeem et al. (2016a)). Every one of these changes acted to corroborate and strengthen the paper's central conclusion, that for these cases carefully processed CML rainfall matches or outperforms the operational RAD-QPE product. We summarize six overarching changes to the revised manuscript that affect several of the responses below:

(1) Quality re-assessment of the disdrometers and revision of all results. During the revision we performed an additional quality assessment of the three disdrometers used to derive the local attenuation-rainfall (γ-R) relations. The instrument located at Uccle exhibited suspicious behaviour: more than half of the values of its velocity-diameter matrix fell outside the range expected from the Gunn-Kinzer terminal fall-velocity relation, and consultation with the responsible RMI staff members indicated that the instrument likely requires recalibration. We therefore omitted this disdrometer and refitted the power-law coefficients using the two remaining instruments (the OTT Parsivel^2 at Melle and the Thies Laser Precipitation Monitor at Liège), while the entire disdrometer processing chain was upgraded to the standardized DISDRODB framework (Ghiggi et al., 2026). All CML rainfall estimates and evaluation statistics in the revised manuscript have been recomputed accordingly. The revised relations predict a higher rain rate than ITU for a given specific attenuation throughout the light-rain range, where the observations are most numerous, and a lower rain rate only at the heaviest rates; the crossover intensity and the magnitude of this difference both increase with frequency, so the largest departures occur for the E-band links and in the light-rain regime (Fig. 4 and Table 4 of the revised manuscript).

(2) A more consistent formulation of the attenuation–rain-rate relation, fitted directly in the retrieval direction and with two objective functions. Acting on Comment 2.20 below, we found that our original comparison with Overeem et al. (2016a) differed from their approach in two respects: they fitted the inverse R–γ relation with an unweighted non-linear least-squares fit, whereas we had fitted the γ–R relation in log–log space. Neither the direction of the regression nor the objective function was therefore matched, and a meaningful comparison required us to reproduce both choices. We now fit the relation directly in the retrieval direction, $R = \mathrm{a} \cdot \gamma^{\mathrm{b}}$, and invert it analytically to the attenuation form ($a' = \mathrm{a}^{-1/\mathrm{b}}, \quad b' = 1/\mathrm{b}$) that pycomlink and the ITU recommendation expect, so that the comparison with Overeem et al. (2016a) is now direct. Repeating the fit with both objective functions turned out to be more than a formality: the two estimators are optimal under different assumptions about the error structure, and their coefficients diverge substantially at the lowest and highest frequencies, where the non-linear fit is dominated by the rare high-intensity samples and is markedly less reproducible between the two disdrometers. Once the same estimator as Overeem et al. (2016a) is adopted, the Belgian and Dutch coefficients at 10 GHz agree closely, which indicates that apparent differences between locally fitted relations reported in the literature can be dominated by the fitting choices rather than by climatology. Both fits are therefore retained as the L and N factor levels of the full evaluation (Table 2), and the role of the objective function is now discussed explicitly in Sect. 4.4. We additionally verified that the regression direction alone (fitting γ–R and inverting, versus fitting R–γ directly) changes the retrieved rainfall only marginally, well below the effect of the objective function.

(3) An α-weighting of the minimum and maximum rain rates to account for sub-window skewness, following Overeem et al. (2016a). Because rainfall within a 15-minute window is typically strongly skewed, a rate retrieved from the window-averaged attenuation misrepresents the mean. We therefore apply the wet–dry classification, the wet-antenna correction and the R–γ inversion consistently to both attenuation envelopes and combine the resulting minimum and maximum rain rates as a weighted average with $\alpha = 0.33$, as in Overeem et al. (2016a). Retrieving instead from the linearly averaged TRSL gave systematically poorer agreement with the reference.

(4) Redesign of the experiment set as a full factorial, and removal of methods developed for 30-second data. Two methods developed for 30-second instantaneous data have been removed: the rolling standard-deviation wet-dry classification of Schleiss and Berne (2010) and the time-dependent wet-antenna scheme of Schleiss et al. (2013), both of which rely on time scales and thresholds that do not apply to the 15-minute MINMAX format of our dataset. Instead, the physically based, frequency- and intensity-dependent wet-antenna model of Leijnse et al. (2008) was added. The retrieval permutations are now organised as a complete 2 x 3 x 3 factorial of the wet-dry classification (nearby links; radar-based), the wet-antenna correction (constant; intensity-dependent; frequency- and intensity-dependent) and the γ-R relation (ITU; Belgian non-linear fit; Belgian log-log fit), giving 18 retrievals per case with a systematic three-letter naming convention (Table 2 of the revised manuscript). This design allows the isolated (marginal) effect of every processing choice to be quantified (Table 6 of the revised manuscript) and resolves the naming ambiguities identified by the reviewer.

(5) A new evaluation-metrics subsection. Sect. 3.6 of the revised manuscript now defines every evaluation metric with an explicit formula: the mean bias (with sign convention: estimate minus reference), the relative bias, the RMSE, the Pearson correlation coefficient r, the coefficient of determination R^2 (computed with respect to the 1:1 line) and the Kling-Gupta efficiency (KGE), which is adopted as the combined ranking metric, together with the matching rules between gauges, CML and RAD-QPE, and the sample sizes entering each comparison. This addresses several of the reviewer's remarks at once (Comments 2.3, 2.6, 2.12, 2.13 and 2.15 below).

(6) A new per-step evaluation of the processing chain (requested jointly with Reviewer 1) has been added, including a two-dimensional sensitivity analysis of the outlier filter, a contingency-table evaluation of the wet-dry classifications, a simplified wet-antenna time-series figure replacing former Fig. 6 (now Figure 3), a CML frequency-and length based performance skill assessment, and a quantification of the minimum detectable rain rate implied by the 1 dB quantization. The Discussion has furthermore been restructured into three subsections (comparison with previous nationwide retrievals; assumptions and limitations; operational implications).

General comments

Comment 2.1. *The summary should be slightly modified as the following wording is confusing: "whether CML-derived rainfall can complement existing dense rain gauge and weather radar network". This is not estimated. And the following wording is excessive: "These findings provide strong evidence that integration of CML information into multi-source precipitation products could yield substantial improvements in high-resolution QPE". This is not demonstrated in the paper.*

Response: We agree on both comments. The first sentence of the abstract now describes what is actually done: *"This study presents the first comprehensive evaluation of rainfall retrievals from a commercial microwave link (CML) network in Belgium against a dense rain gauge and weather radar network."* The closing sentence has been toned down accordingly: *"These findings suggest that integration of CML information into multi-source precipitation products may yield improvements in high-resolution QPE, particularly for urban hydrological applications and extreme-event monitoring."*

Changes to the manuscript: Abstract, first and last sentences rephrased; the corresponding overstatement in the Discussion has been rephrased as well (see our response to Comment 2.17).

Comment 2.2. *Since the data processing relies on the free software pycomlink, there are not really any new concepts or methods, apart from the use of disdrometer data to estimate specific attenuation-rainfall rate relationships (although this has already been done). The data describes four extreme rainfall events of 24h or 48h (i.e. 7 days), all within a period of 38 days in summer 2023, which is a quite limited diversity in hydrometeorological situation.*

Response: We acknowledge both points explicitly in the revised manuscript. Regarding the event sample, the Discussion now states: *"Regarding the event sample, four cases within a single summer represent a limited range of hydrometeorological conditions, and the results should not be extrapolated to light or cold-season precipitation, which is known to be more demanding for CML retrievals (Overeem et al., 2016b)."* (Sect. 5.2, final paragraph), and extension to a multi-year record covering stratiform and winter situations is identified as future work.

Regarding the methodological contribution, we agree that the individual building blocks originate from the literature and are largely available in pycomlink, and the revised manuscript states this openly. At the same time, the revision has considerably deepened the elements that are, to our knowledge, new: the complete 2 x 3 x 3 factorial evaluation of processing permutations against a dense operational gauge network and a national radar QPE, including the marginal effect of each individual processing choice (Tables 5 and 6); a formalised, variogram-based spatial outlier filter with a two-dimensional sensitivity analysis of its parameters (Sect. 3.2, Fig. 2); a quantification of the minimum detectable rain rate implied by the 1 dB quantization for every link of the network (Fig. 5); locally derived γ-R relations for Belgium obtained with two fitting objectives, showing that the fitting strategy alone can explain a substantial part of apparent inter-study differences in published relations (Sect. 4.4, Table 4); and the first evaluation of an E-band-dominated urban subnetwork at 15-minute resolution against fully independent gauges (Sect. 4.6). We have sharpened the framing of the contribution along these lines in the Introduction and Conclusions.

Changes to the manuscript: Sect. 5.2 (limitations of the event sample); Introduction and Conclusions reframed; new analyses as listed above.

Comment 2.3. *Also, some criteria should be presented more explicitly (with formulas and definition of the values compared), and in general, the authors should verify that all abbreviations or variable names are correctly defined before use. May be a short sub-section could be useful in section 3 (Method) to define the validation methodology and the calculation of the criteria used.*

Response: This suggestion has been adopted. A new subsection "Evaluation Metrics" (Sect. 3.6) defines every criterion with an explicit formula: the mean bias (Eq. 11, with sign convention estimate minus reference), the relative bias, the RMSE (Eq. 12), the Pearson correlation coefficient r (Eq. 13), the coefficient of determination R^2 (Eq. 14, computed with respect to the 1:1 line) and the Kling-Gupta efficiency (Eq. 15), which is used as the combined metric for ranking the permutations. The subsection also specifies the value pairs entering each comparison: the CML-gauge and RAD-QPE matching rules, the temporal alignment, and the sample sizes, which are additionally reported in every evaluation table. The rain gauges actually used in the detailed gauge-referenced evaluation are also highlighted in the network maps in Figure 1. All abbreviations and variable names have been checked for definition at first use.

Changes to the manuscript: New Sect. 3.6: *Throughout this study, the CML-derived rainfall estimates (and, where relevant, RAD-QPE) are evaluated against the rain gauge measurements. Denoting the rainfall estimates by S_i and the reference observations by O_i ($i = 1, \ldots, n_{sam}$), with overbars indicating averages over all n_{sam} samples, the following statistical metrics are used. The mean bias,*

$$\text{Bias} = \frac{1}{n_{sam}} \sum_{i=1}^{n_{sam}} \left(S_i - O_i\right), \tag{1}$$

quantifies the systematic over- or underestimation of the reference; the relative bias is the mean bias normalised by $\bar{O}$. The root-mean-square error,

$$\text{RMSE} = \sqrt{\frac{1}{n_{sam}} \sum_{i=1}^{n_{sam}} \left(S_i - O_i\right)^2}, \tag{2}$$

measures the typical magnitude of the estimation errors and is dominated by the largest deviations. The strength of the linear association between estimates and reference is expressed by the Pearson correlation coefficient,

$$r = \frac{\sum_{i=1}^{n_{sam}} \left(S_i - \bar{S}\right)\left(O_i - \bar{O}\right)}{\sqrt{\sum_{i=1}^{n_{sam}} \left(S_i - \bar{S}\right)^2}\sqrt{\sum_{i=1}^{n_{sam}} \left(O_i - \bar{O}\right)^2}}, \tag{3}$$

which is insensitive to systematic biases and to differences in variability. The overall agreement with the reference is therefore additionally quantified by the coefficient of determination,

$$R^2 = 1 - \frac{\sum_{i=1}^{n_{sam}} \left(S_i - O_i\right)^2}{\sum_{i=1}^{n_{sam}} \left(O_i - \bar{O}\right)^2}, \tag{4}$$

computed with respect to the 1:1 line rather than a fitted regression, equivalent to the Nash–Sutcliffe efficiency. In this form, R^2 penalises both random and systematic errors, equals one for a perfect estimate, and can become negative when the estimates perform worse than the reference mean.

Finally, the Kling–Gupta efficiency (Gupta et al., 2009) is used as a combined metric,

$$\mathrm{KGE} = 1 - \sqrt{(r-1)^2 + (\alpha_{KGE}-1)^2 + (\beta_{KGE}-1)^2}, \tag{5}$$

where r is the Pearson correlation of Eq. 3, $\alpha_{KGE} = \sigma_S/\sigma_O$ is the ratio of the standard deviations of the estimates and the reference, and $\beta_{KGE} = \bar{S}/\bar{O}$ is the ratio of their means. The KGE thus penalises errors in correlation, variability and bias simultaneously, with $\mathrm{KGE} = 1$ indicating a perfect estimate. Because it condenses these three complementary aspects of retrieval quality into a single score, the KGE is used whenever one scalar skill measure is required, in particular for the selection of the outlier-filter parameters in Section 3.2 or to rank the different processing permutations in Sect.4.5.; sample sizes added to relevant Tables and Figures.

Specific comments - inconsistencies

Comment 2.4. *First confusion in 2.4 Radar Data. Radar data is described as an operational state-of-the-art radar-gauge merged product. In Journée et al. (2023) we find: "Instantaneous rain rates are obtained every 5 min, corresponding to the full 3D radar scan. The rainfall accumulation over 5 min is obtained by computing the movement of precipitation using optical flow techniques." But in the 2.4 section, the authors write "(aggregating the three 5-minute values, without taking into account advection over a 5-minute interval)". This is confusing because: - it is not necessary if the advection is already done in the 5-minute radar QPE computing. - if the radar-based 15-minute QPE not include advection, this QPE is not state-of-the-art. Please clarify.*

Response: We thank the reviewer for spotting this poorly worded section. The operational 5-minute accumulations of RAD-QPE do include optical-flow-based advection, as described by Journée et al. (2023). Our sentence was only meant to state that the three 5-minute accumulations are summed to obtain 15-minute accumulations, and that no additional advection correction is applied, or needed, at that aggregation step. The section has been rewritten accordingly.

Changes to the manuscript: Sect. 2.4: *"The product used in this study is the 5-minute accumulation product (which takes into account advection using optical flow techniques), which was aggregated to 15-minute frequency to maintain consistency with the sub-hourly resolution of the other rainfall products employed."*

Comment 2.5. *Second confusion about best WAA correction. In the summary and in section 5 (line 440), rainfall-intensity-dependent wet-antenna correction is presented as the best option, which is in accordance with several results in literature, but in section 4.3 (line 371) the authors write "RII appears to have the worst metrics of the three wet-antenna correction method" (so why to us it in RID version?). Please clarify. Remark: the RII "correlation" is the best for "all cases" except radar and RID (table 5).*

Response: The reviewer identified a genuine inconsistency, which arose because the original acronyms did not isolate a single processing choice: RII and RID shared the same (intensity-dependent, Pastorek et al. (2022)) wet-antenna correction and differed only in the R–γ relation (ITU versus the Belgian disdrometer fit), so a statement that "RII has the worst metrics of the three wet-antenna corrections" and the choice to use the intensity-dependent correction in the best-performing RID could appear to contradict one another, even though the difference between the two permutations was due to the R–γ relation and not the wet-antenna method. This has been resolved in the revision: whereas the original manuscript evaluated only a subset of permutations, all 18 combinations of the three processing choices are now run as a complete factorial (Table 2). The three-letter naming is retained, but because every factor is now varied while the other two are held fixed, the effect of the wet-antenna method can be isolated at fixed wet–dry classification and fixed R–γ relation.

The recomputed results also change the substance of the answer. Averaged over all permutations sharing the same wet-antenna method, the constant correction attains the highest marginal KGE (0.76), followed by the frequency- and intensity-dependent Leijnse et al. (2008) method (0.70) and the intensity-dependent Pastorek et al. (2022) method (0.61) (Table 6). However, the revised Sect. 4.3 explains that the strong performance of the constant correction partly reflects error compensation: its abrupt on–off behaviour with a constant (and fairly high) correction suppresses the spurious light rainfall produced by false alarms in the nearby-link wet–dry classification, which the dynamic methods correctly leave in place. When the more accurate radar-based classification is used, combined with the locally fitted relations, the Leijnse et al. (2008) correction performs on par with or better than the constant one, and the overall best permutation is RFL (radar classification, Leijnse et al. (2008) correction, log–log local fit; case-combined KGE 0.85, Table 5).

The reviewer's observation about the correlation of RII remains valid in the recomputed results, and it is in fact diagnostic. RII now ranks twelfth of the eighteen permutations (case-combined KGE 0.70), yet its correlation with the gauges (0.85) is still among the highest of all permutations. The deficiency of the Pastorek et al. (2022) correction in our network is therefore not a loss of covariation with the reference, but a systematic positive bias (+2.4 mm, or 17 %), which the KGE penalises through its bias and variability terms while the correlation coefficient is insensitive to it. The mechanism is visible in the new wet-antenna time-series figure (Fig. 3), which contrasts a low-frequency and a high-frequency link: at the high-frequency link and at moderate rain rates, the Pastorek et al. (2022) correction is smaller than both the constant correction of Overeem et al. (2016a) and the frequency-dependent correction of Leijnse et al. (2008), so that too much of the observed attenuation is attributed to rainfall. This is consistent with the fact that its coefficients were calibrated on links operating between roughly 24 and 38 GHz and contain no explicit frequency dependence, so their application to an E-band-rich network is an extrapolation. The abstract, Sect. 4.3, the Discussion and the Conclusions have been checked for consistency with these recomputed numbers.

Changes to the manuscript: Naming convention redesigned (Table 2); Sect.4.3 rewritten; marginal effects in Table 6; ranking in Table 5 and the supplement.

Comment 2.6. *Third confusion. The validation use two related criteria: - The coefficient of determination (R2) - The "correlation" (r). Please clarify if r is the Pearson correlation coefficient, and clarify the calculation of r and R2 (formula, values used), and explain the large differences of values between R2 and r2 when you compare two sets of rainfall values.*

Response: r is indeed the Pearson correlation coefficient, and both metrics are now defined with explicit formulas in the new Sect. 3.6 (Eqs. 13-14), computed on the same value pairs. R^2 is the coefficient of determination computed with respect to the 1:1 line rather than the regression line; the revised text states: *"In this form, R^2 penalises both random and systematic errors, equals one for a perfect estimate, and can become negative when the estimates perform worse than the reference mean."* The two metrics therefore only coincide ($\mathrm{R}^2 = \mathrm{r}^2$) for an unbiased linear fit; because several CML permutations carry substantial bias and amplitude errors, R^2 falls well below r^2 for these, which is precisely the diagnostic value of reporting both. This explanation is now given where the metrics are introduced, and the Kling-Gupta efficiency, which combines the disagreement in correlation, bias and variability terms, has been added as the combined ranking metric.

Changes to the manuscript: New Sect. 3.6 (Eqs. 13-15).

Specific comments - remarks

Comment 2.7. *Please define a "sublink" (page 4, line 81).*

Response: A definition has been added at first use in Sect. 2.2: *"over 1600 CMLs (comprising about 2800 sublinks, denoting one directed transmission channel of a link; each physical CML path typically comprises two sublinks operating in opposite directions)"*.

Comment 2.8. *Could you explain the impact of ATPC on attenuation estimation? (page 4)*

Response: Automatic transmit power control (ATPC) adjusts the transmitted power to maintain the received level during strong attenuation. Because the dataset records both transmitted and received signal levels, these adjustments are accounted for in the total received signal loss used in our processing. The new Sect. 3.1 now explains this explicitly: two TRSL extremes are constructed from the reported TSL and RSL extremes, TRSL_max = TSL_max - RSL_min and TRSL_min = TSL_min - RSL_max (Eq. 1), exploiting the anti-correlation between transmitted and received levels under ATPC. ATPC therefore does not bias the attenuation estimate systematically, but the minima and maxima of TSL and RSL within a 15-minute interval are not necessarily simultaneous, so that ATPC activity can add a non-systematic uncertainty; the revised text acknowledges this: *"We do acknowledge that this causes some uncertainty, since it is likely that there is a time lag between the occurrence of the minimum (maximum) TSL and maximum (minimum) RSL."* The same assumption also affects the nearby-link wet-dry classification, for which the adjustment of Roversi et al. (2020) is applied (Sect. 3.3), and it is listed among the limitations in Discussion Section 5.2.

Changes to the manuscript: Sect. 3.1 (Eq. 1 and accompanying text); Sects. 3.3 and 5.2.

Comment 2.9. *Wet-dry classification: could you explain what you think about estimating standard variation of attenuation using 8 values? The authors write "The advantage of this method is that generally no calibration is needed" I am surprised that this criterion can be used without calibration, because thresholds must be used. Please explain.*

Response: We fully agree with the reviewer, and this comment, together with a similar concern of Reviewer 1, led us to remove the rolling standard-deviation classification from the revised manuscript altogether. A standard deviation estimated from only eight 15-minute samples in a 2-hour window is statistically fragile, and the method does require threshold choices (window length and standard-deviation threshold) that were calibrated on 30-second instantaneous data and do not transfer to the 15-minute MINMAX format; the claim that no calibration is needed was incorrect and has been removed with the method. The revised manuscript retains two wet-dry classifications (nearby links and radar-based), whose skill is now assessed objectively through a contingency-table evaluation against gauge-observed wet and dry states (Sect. 4.2, Table 3).

Changes to the manuscript: Rolling standard-deviation classification removed (Sect. 3.3, Table 2); new contingency evaluation (Sect. 4.2, Table 3).

Comment 2.10. *WAA line 227: the decrease in WAA after the end of the rain: many references indicate that this decrease is highly variable, depending on various factors (including weather conditions). Line 232: Could the authors verify the 14 dB value for an upper limit for WAA? (I cannot access the Leijnse reference)*

Response: With the removal of the Schleiss et al. (2013) scheme (General response, point 4), no post-event decay time constant is used anywhere in the revised manuscript. We fully agree that the antenna drying time is highly variable and depends on weather conditions and antenna properties; this variability is in fact one of the reasons why we prefer not to use time-dependent wet-antenna parameterisations at 15-minute resolution, where a single decay constant of the order of the sampling interval cannot represent it.

We have verified the 14 dB value, and we thank the reviewer for prompting us to attribute it properly. It does not originate from Leijnse et al. (2008), whose physically based wet-film model requires no empirical cap. It is the parameter C of the "KR-alt" wet-antenna model of Pastorek et al. (2022), in which the wet-antenna attenuation is limited by construction:

$$A_{\mathrm{waa}} = C\left(1 - \exp\left(-d\, R^{z}\right)\right),$$

with C [dB] the maximum attenuation the model allows, and d fixed at 0.1 by Pastorek et al. (2022) because C and d are not independent and can compensate for one another. The value of 14 dB is the default for C in the pycomlink implementation, alongside `zeta` $= z = 0.55$ and `d` $= 0.1$), which are the values we adopt.

It is important to note that C is an asymptotic bound approached only as $R \to \infty$, not a value attained at realistic rain rates. With the default parameters the correction amounts to about 1.3 dB at 1 $\mathrm{mm\,h^{-1}}$, 4.2 dB at 10 $\mathrm{mm\,h^{-1}}$ and 10 dB at 100 $\mathrm{mm\,h^{-1}}$. Consistently, the corrections diagnosed in our network are of the order of 2 to 4 dB (Sect. 4.3, Fig. 3), so the upper limit is never active in our retrievals and does not influence the results. What does matter is that these coefficients were calibrated on links operating between roughly 24 and 38 GHz and contain no explicit frequency dependence, so that their application to an E-band-rich network is an extrapolation; this is now stated in Sects. 3.4, 4.3 and (Discussion).

Changes to the manuscript: Sect.3.4 rewritten (Schleiss et al. (2013) scheme removed; Leijnse et al. (2008) model added; the Pastorek et al. (2022) parameters now given with their symbols and attributed correctly, together with the note that C is an asymptotic upper bound); extrapolation caveat added in Sects. 4.3 and 5 (Discussion).

Comment 2.11. *In section 4.1 and figure 4 : Could the authors explain the impact of an ordinary kriging on the validation criteria, particularly the e-folding radius? Reminder: RAD-QPE is the best radar-gauge spatialization, and a simple ordinary kriging of rain gauges measurements is not a state-of-the-art product. It would be interesting to know if the kriging used the same variogram or not for the different estimations.*

Response: The kriging configuration is now stated unambiguously: the ordinary kriging uses the daily-varying climatological spherical variogram of van de van de Beek et al. (2012), i.e. a variogram whose parameters depend on the day of year but not on the individual event, and exactly the same variogram model and parameters are used for the interpolation of the gauge measurements and for the interpolation of the CML retrievals (Sect. 2.3). Differences between the interpolated fields therefore reflect the input data rather than the interpolation settings. We also clarify that the e-folding lengths λ reported in the panels of the map figure (Fig. 6) are diagnostic spatial autocorrelation lengths of the resulting accumulation fields, computed a posteriori to characterise their spatial structure; they are not parameters of the kriging itself (but of course will be influenced by the interpolation method). This is now stated in the caption.

We agree that a plain ordinary kriging of the gauges is not a state-of-the-art product, and the revised text presents it accordingly: it serves as an availability baseline that shows what the operational gauge network alone can resolve, against which the added value of RAD-QPE (acknowledged as the reference spatialization) and of the CML fields can be judged. We further note that the quantitative evaluation (Tables 5 and 8) is performed at the gauge locations on the un-interpolated estimates, so the kriging influences only the qualitative map comparison, not the validation criteria.

Changes to the manuscript: Sect. 2.3 (variogram specification); caption of Fig. 6 (λ as diagnostic); Sect. 4.5 (role of the kriged gauge product).

Comment 2.12. *In table 5: Please, define the bias formula: "CML estimate minus reference" or "reference minus CML estimate"?*

Response: The bias is defined as the estimate minus the reference, so positive values indicate CML (or radar) overestimation of the gauges. This is now given as an explicit formula (Eq. 11) in the new Sect. 3.6 and applies to every table reporting a bias.

Comment 2.13. *Line 371 and figure 5: RII results surprises me. Please, verify the determination R2 values and the values compared for each criterion (see above remarks)..*

Response: All values have been recomputed for the revised manuscript (with the refitted R–γ relations and the redesigned permutation set), and the calculation of every metric, including R^2, is now defined explicitly with the exact value pairs and sample sizes (Sect. 3.6; see our response to Comment 2.3). The RII permutation still exists in the revised factorial, but its position has changed with the new processing chain: it now ranks twelfth of the eighteen permutations for the case-accumulated evaluation, owing to a positive bias in the retrieved rainfall (Table 5 and the complete ranking in the supplement). The mechanism is visible in the new wet-antenna time-series figure (Fig. 3), which contrasts a low-frequency and a high-frequency link: at the high-frequency link and at moderate rain rates, the intensity-dependent correction of Pastorek et al. (2022) is smaller than both the constant correction of Overeem et al. (2016a) and the frequency-dependent correction of Leijnse et al. (2008), so that more of the observed attenuation is attributed to rainfall. This is consistent with the fact that the Pastorek et al. (2022) coefficients were derived for links operating between roughly 24 and 38 GHz and contain no explicit frequency dependence, so their application to an E-band-rich network is an extrapolation. The apparent inconsistency in the interpretation of RII noted by the reviewer is separately resolved by the completed factorial and the rewritten wet-antenna comparison, as detailed in our response to Comment 2.5.

Comment 2.14. *Line 375: Remark: The authors write "It should be mentioned that the constant value of 2.3 dB could in principle be reduced in RCI and RTI, particularly during light rain, to allow more light rain to be detected". Have you a concrete method to do that?*

Response: The concrete mechanism is precisely what the dynamic wet-antenna schemes provide: both the Pastorek et al. (2022) and the newly added Leijnse et al. (2008) methods reduce the wet-antenna attenuation towards zero for small observed attenuations, i.e. during light rain, in an empirically or physically constrained way. We therefore do not attempt an ad hoc tuning of the 2.3 dB constant, which is retained only as a simple and widely used baseline. The speculative sentence has been removed; the revised Sect. 4.3 instead contrasts the behaviours directly: *"Because Overeem et al. (2016a) assigns a fixed A_waa of 2.3 dB to every wet time step irrespective of intensity, its correction switches on and off abruptly with the wet-dry classification, whereas the dynamic methods increase A_waa from near zero as the attenuation grows."*

Changes to the manuscript: Sect. 4.3 rewritten around the new Fig. 3.

Comment 2.15. *Figure 7: same remark as before: How R2 and r values have been calculated?*

Table 6: could you more explain the differences between "mean rate" and "mean intensity"? With or without zero values?

Response: All metrics shown in the figures and tables are computed as defined in the new Sect. 3.6, and each caption now states the sample size. For the table of gauge statistics over the Brussels-Capital Region (Table 7 of the revised manuscript), the caption now defines both quantities explicitly: *As Table 1, but for the IBGE network only, and including the average rain rates. Shown are the domain-average rain rate (*$\mathrm{mm\ h^{-1}}$*), averaged over all 15-min intervals of the case, including the dry ones; the domain-average intensity (*$\mathrm{mm\ h^{-1}}$*), averaged over the wet intervals only, that is, conditional on rainfall being recorded; the case-total accumulation (mm) and the case-accumulated 99th percentile (mm) and standard deviation (mm). The mean rate therefore reflects both the intensity and the temporal occurrence of rainfall, whereas the mean intensity characterises the rainfall when it occurs.* The former Fig. 7 has been replaced by the per-link frequency x length skill evaluation (Fig. 7), whose caption lists the metrics shown in each frequency–length cell.

Changes to the manuscript: Sect. 3.6; caption of Table 7; new Fig. 7.

Comment 2.16. *Remark lines 446-447: The authors write "It should also be mentioned that considerable uncertainty on the wet-antenna correction exists due to the fact that both antennas of a CML are not necessarily wet at the same time, particularly during scattered shower." Why not use radar data for that?*

Response: This is an interesting suggestion. Radar data could indeed be used to diagnose whether rainfall occurs at either antenna location (for instance from the radar pixels containing the two endpoints) and to modulate the wet-antenna correction accordingly. We considered discussing this at length, but implementing and validating such a radar-informed scheme is beyond the scope of this study and would inflate the manuscript size (while it has already become longer than the first version), and several caveats would need to be resolved first: the uncertainty of radar rain detection at the pixel scale (the very reason the wet-dry classification uses a path-integrated criterion), the mismatch between the 15-minute resolution and the antenna wetting and drying time scales, and the fact that endpoint rainfall does not capture dew or residual water films on the antenna. The revised Discussion retains the limitation itself, noting that *"any single-valued correction is at best an expectation over both ends of the path"*, and identifies the local calibration of the wet-antenna model on the dense Belgian gauge network, following Valtr et al. (2019) and Pu et al. (2020), as the most promising avenue for improvement (Sect. 5.2).

Changes to the manuscript: Sect. 5.2 (limitation retained and future avenues identified).

Comment 2.17. *Line 465: The authors write "our results provide evidence that existing multi-modal rainfall products could be substantially improved through integration of CML information that can be accessed in real time." No. They haven't tried to merge CML data with other data, so the results not really "provide evidence" on the matter.*

Response: We agree and have rephrased the claim throughout. The corresponding abstract sentence has been toned down (see our response to Comment 2.1), and the Discussion now states the implication conditionally, without claiming demonstrated merging skill: *"This does not make CMLs a substitute for radar, whose spatial coverage is complete and whose performance does not depend on the local density of telecommunication infrastructure, nor for gauges, which remain necessary for validation and adjustment. It does, however, make CML retrievals a credible third component of a multimodal product, particularly over urban areas."* The revised text adds explicitly that how best to merge the three sources, and how much skill such a merged product would gain, is left for future work.

Changes to the manuscript: Abstract and Sect. 5.3 rephrased.

Technical corrections

Comment 2.18. *For equation (4) and (5) , define Di, ND, NV*

Response: Definitions have been added below the corresponding equations (Eqs. 8-10 of the revised manuscript): Δt is the sampling interval, D_i and ΔD_i the centre and width of diameter bin i, n_ij the number of drops counted in diameter bin i and velocity bin j, V_j the fall velocity of velocity bin j, A_eff(D_i) the diameter-dependent effective sampling area of the instrument, and N_D and N_V the numbers of diameter and velocity bins of the disdrometer.

Comment 2.19. *line 258 "polarisation pol" and not "polarisation p"*

Response: Corrected; the subscript now reads pol throughout Sect. 3.5.

Comment 2.20. *Table3. Can the authors provide the Overeem et al. (2016a) values?*

Response: Yes, and we are grateful for this request, because acting on it led to one of the more interesting findings of the revision. When we retrieved the coefficients of Overeem et al. (2016a) in order to add them, we realised that they had been obtained by fitting the inverse R-γ relation with a non-linear least-squares approach, whereas we had originally fitted the γ-R relation linearly in log-log space. Since the direction of the regression and the choice of estimator both matter, the comparison was not like for like, and we therefore returned to our disdrometer data and now fit the relation directly in the retrieval (R-γ) direction, with both fitting functions, reporting these throughout and inverting analytically to the attenuation form that pycomlink expects. This revealed that the choice of fitting procedure matters considerably, in some respects more than the climatological difference the comparison was originally meant to expose.

The effect is clearest at the lowest frequencies. Expressed in the inverse form that is directly comparable with Fig. 2 of Overeem et al. (2016a), our log-log fit at 10 GHz gives a prefactor of 60.2, which differs markedly from the Dutch value of 37.7. When the same class of estimator as Overeem et al. (2016a) is adopted, however, the Belgian coefficients move close to the Dutch ones (prefactor 39.5 and exponent 0.75, against 37.7 and 0.75). Given the similarity of the two climates, this agreement is reassuring, and it indicates that apparent inter-study differences in locally fitted relations at low frequencies can be dominated by the fitting procedure rather than by genuine differences in drop size distributions. The revised manuscript draws the corresponding methodological conclusion that this choice should be reported explicitly whenever locally fitted relations are compared.

The two estimators also behave differently in a way that matters for which one to use. The non-linear fit is more affected by the few most intense minutes in the record, which sample different individual storms at our two disdrometer sites and fall precisely in the intensity range where optical disdrometers of different designs are known to disagree most (Angulo-Martínez et al., 2018). Accordingly, the non-linear fits of the Melle and Liège instruments diverge substantially at the low frequencies (in the retrieval R–γ form, prefactors of 40.4 versus 31.8 at 10 GHz), whereas their log-log fits agree closely at all frequencies (exponents of 0.86 versus 0.88 at 10 GHz and 1.08 versus 1.07 at 80 GHz). The log-log objective draws on the full intensity distribution rather than allowing the extremes alone to determine the residuals, and therefore yields relations that are more reproducible across instruments, which we consider the more appropriate property for coefficients intended to be applied to an entire national network. We have not, however, treated this as settled: both fits are now reported side by side in Table 4, both are carried through the full evaluation as separate factor levels of the factorial design (the L and N levels of Table 2), and the retrievals are compared against the gauges for each. Because we now fit the relation directly in the retrieval (R–γ) direction, we also verified the reverse choice (fitting the γ–R relation and inverting it) and found that the impact of the regression direction is smaller than that of the fitting strategy.

Table 4 of the revised manuscript now lists the ITU recommendation, both Belgian fits and the Netherlands values of Overeem et al. (2016a) in the retrieval (R–γ) form, at 10, 25 and 80 GHz, so that readers can make the comparison directly; the attenuation-form coefficients follow by the analytic inversion $a' = \mathrm{a}^{-1/\mathrm{b}}, \quad b' = 1/\mathrm{b}$.

Comment 2.21. *Figure 5: In the legend: "and (b-i) all permutation", may be (b-h)?; Title graph RII and RTI seems inverted; Is it possible to better define the 453 compared values?*

Response: The former Fig. 5 has been replaced in the revision: the accumulation comparison of all permutations is now reported as a ranking table of the five best permutations per case and case-combined (Table 5), with the complete ranking of all 18 permutations in the supplement (Table 10). The legend and panel-title issues therefore no longer arise. The composition of the compared values is now defined explicitly: each case contributes the gauges with at least one CML midpoint within 2.5 km (83 to 103 gauges depending on the case), giving 387 station-case pairs for the case-combined statistics; these sample sizes are reported in the tables.

Comment 2.22. *Figure 6: overlapping lines make the figures not very legible. Some lines are not visible. Try to improve it.*

Response: The figure has been replaced entirely (new Fig. 3), also following a suggestion by Reviewer 1. The new figure shows a single representative event and separates the overlapping information a bit more into distinct panels: the TRSL with the retrieved baseline, the wet-antenna attenuation of each method in its own colour, and the resulting rain rates, with shading marking the intervals classified as wet and with dry periods before and after the rainfall included. One low-frequency and one high-frequency link are shown to illustrate the frequency dependence of the newly added Leijnse et al. (2008) correction.

Comment 2.23. *Figure 10: Please, change the colour of dots (not legible), particularly blue/green and red/purple*

Response: The former Fig. 10 has been replaced by a ranking table of the 15-minute evaluation over the Brussels-Capital Region (Table 8, with the complete ranking in Table 11), so the colour issue no longer arises there. The former Fig. 10 scatter plots no longer appear; the replacement Fig. 7 is a frequency x length skill grid whose colour scales (a diverging scale for bias and a perceptually uniform scale for RMSE and KGE) we have checked for legibility, including for colour-vision deficiencies.

We once more thank the reviewer for the careful and constructive review, which helped us to remove several genuine inconsistencies and to make the evaluation methodology fully explicit.

1 Figures

Note that original Figure 2 was removed, since the frequency-length distribution is now shown in Figure 7a and b for a representative sample of links.

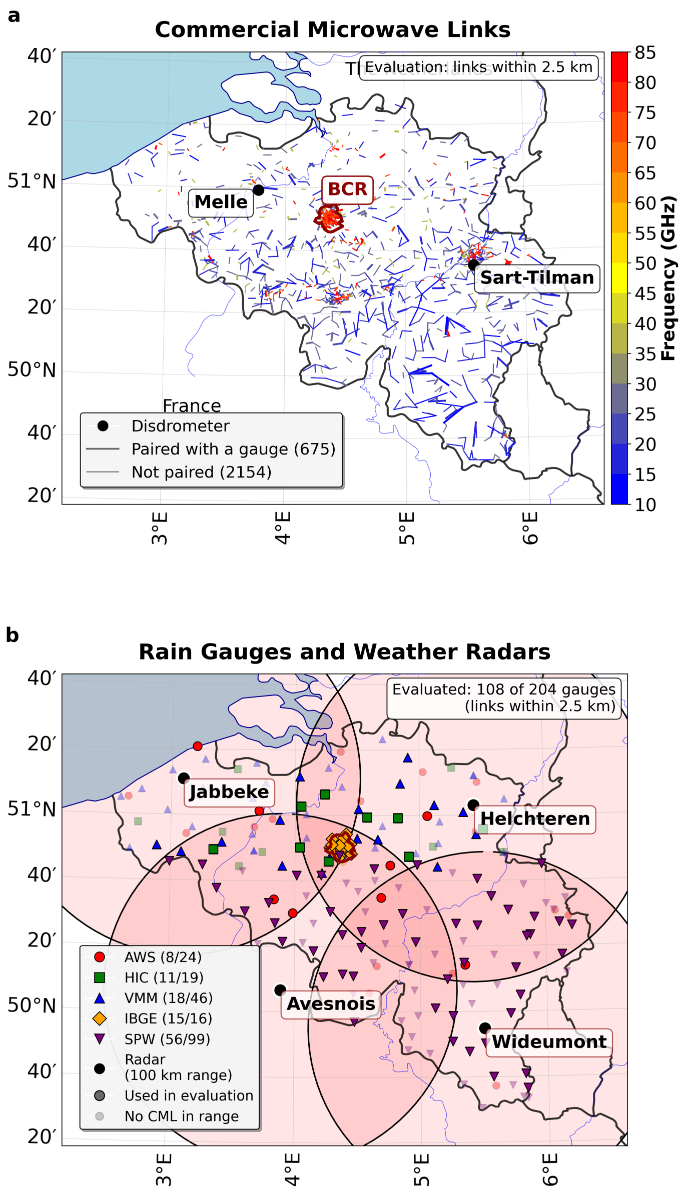

Figure 1: Spatial distribution of (a) CML network and disdrometers and (b) rain-gauge and weather radar networks in Belgium as used in this study. The colors of the CMLs reflect their operating frequency. The rain-gauge networks have different symbols as outlined in the legend. A 100 km radius around each radar site is shown by the black circles. The red outline of the Brussels-Capital Region (BCR) is also shown, for reference (see Section 4.6).Rain gauges highlighted in (b) are within 2.5 km of a CML midpoint, and are the ones used in the more detailed evaluation of CML-rainfall permutations and RAD-QPE

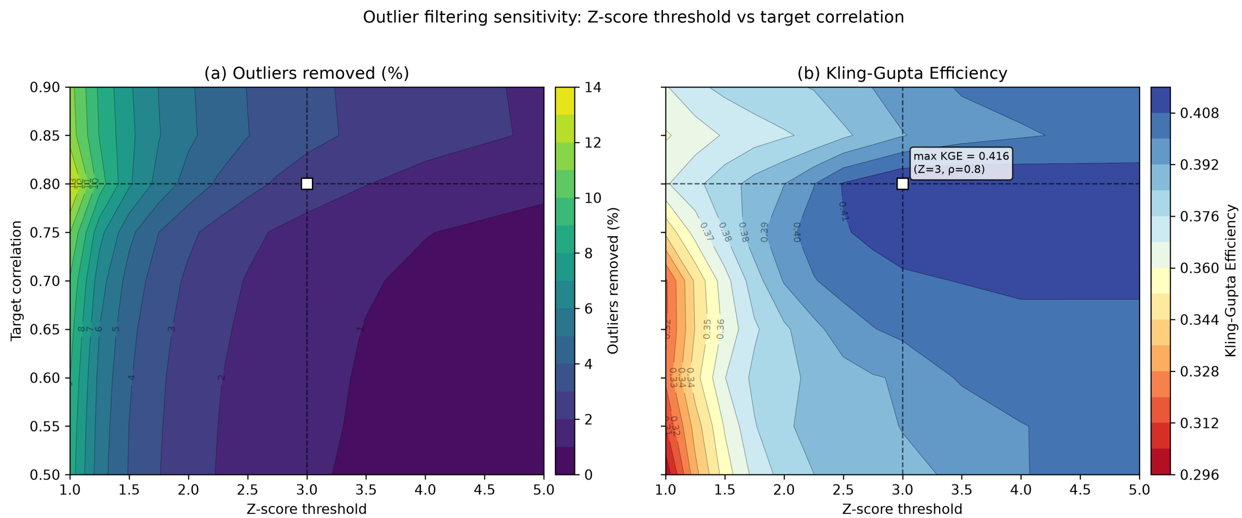

Figure 2: Sensitivity of the outlier filter (Section 3.2) to the Z-score threshold Z_{thr} and the target correlation ρ^*: (a) percentage of 15-min link samples removed and (b) Kling–Gupta efficiency (Equation 15) of the retrieved 15-min rainfall evaluated against the rain gauges. Both quantities are averaged over all four cases and all 18 processing permutations (72 retrieval runs). The white square and dashed lines mark the selected combination ($Z_{\mathrm{thr}} = 3$, $\rho^* = 0.8$), for which the mean KGE reaches its maximum of 0.416.

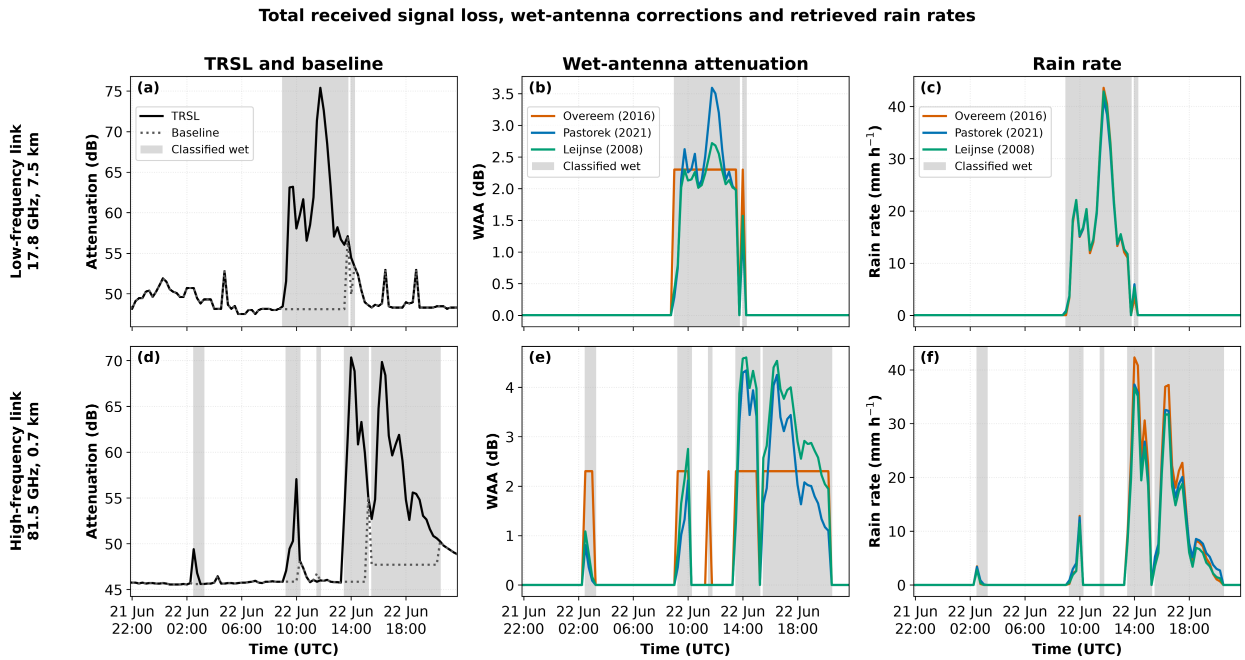

Figure 3: Time series for a low-frequency link (17.8 GHz, 7.5 km; top row) and a high-frequency link (81.5 GHz, 0.7 km; bottom row) for Case 1. Shown are (a, d) the total received signal loss (TRSL) and the retrieved baseline attenuation A_{dry}, (b, e) the wet-antenna attenuation A_{waa} and (c, f) the retrieved 15-min rain rates, for the constant correction of Overeem et al. (2016a) (·C·, orange), the intensity-dependent correction of Pastorek et al. (2022) (·I·, blue) and the intensity- and frequency-dependent correction of Leijnse et al. (2008) (·F·, green). Grey shading indicates the intervals classified as wet by the radar-based classification, which is shared by all three permutations.

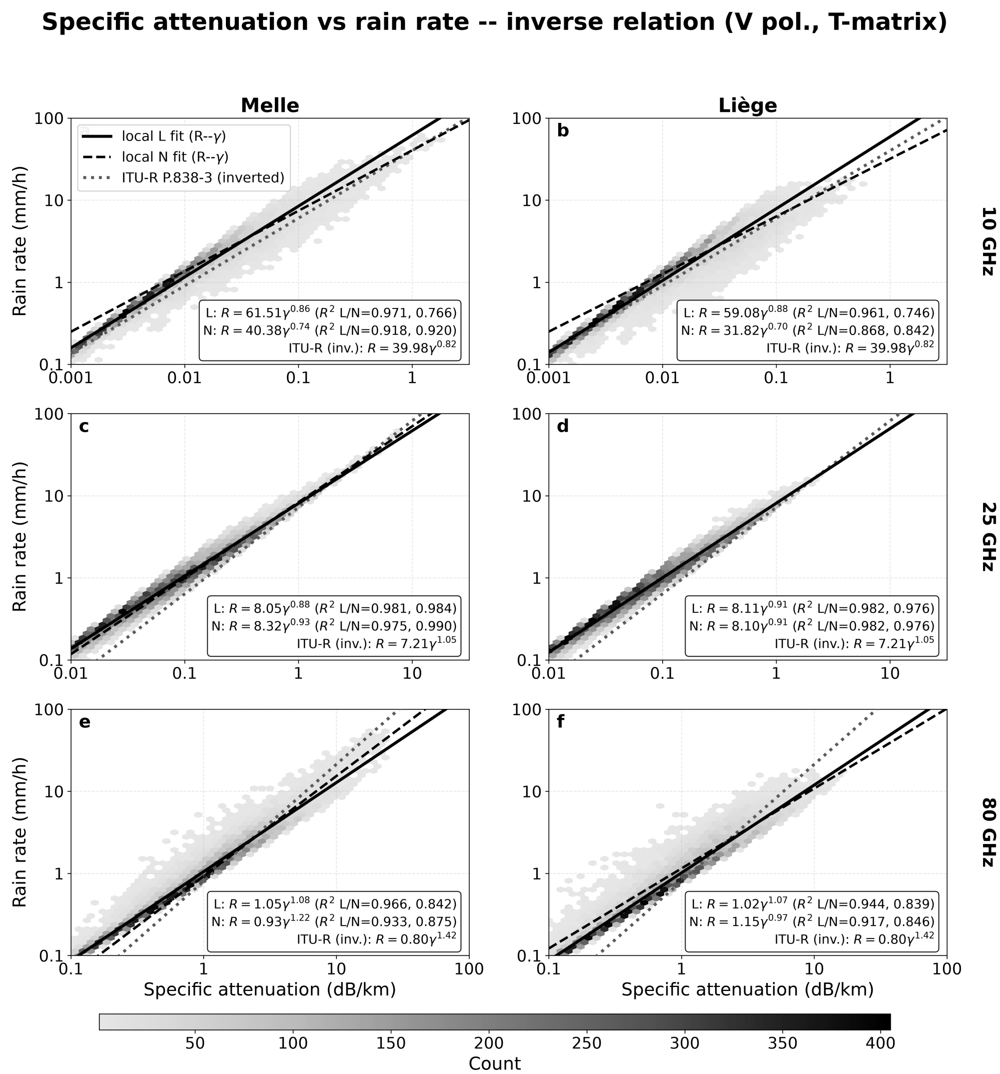

Figure 4: Rain rate as a function of specific attenuation for the (left) Melle and (right) Liège disdrometers at (top) 10 GHz, (middle) 25 GHz and (bottom) 80 GHz, assuming vertical polarization, based on the one-minute observations of May–September 2024 and 2025. The greyscale indicates the number of observations per bin. The dotted line shows the inverted ITU relation (ITU, 2005), the dashed line the local non-linear fit and the solid line the local fit in log–log space, all in the retrieval direction $\mathrm{R} = \mathrm{a}\,\gamma^{\mathrm{b}}$. The boxes list the fitted coefficients of both local relations, with their coefficients of determination evaluated in logarithmic and in linear space, together with the inverted ITU relation. Note the different X-axis ranges for each frequency.

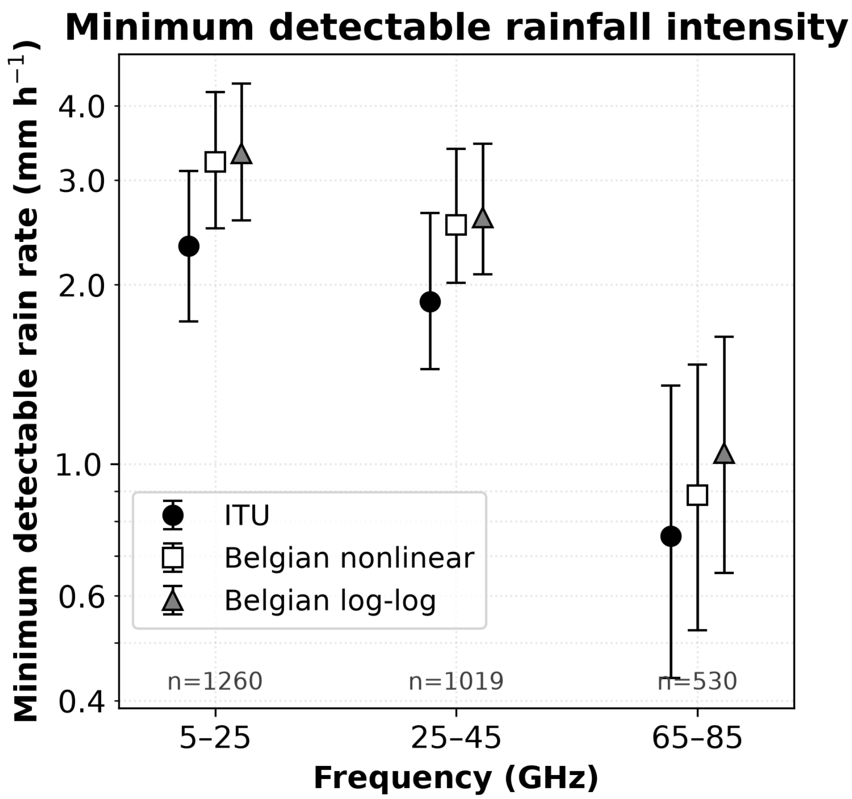

Figure 5: Minimum detectable rain rate implied by the 1 dB quantization of the network management system, computed for each individual sublink as $R_{\min} = (\Delta A_{\mathrm{q}}/(a'L))^{1/b'}$, with $\Delta A_{\mathrm{q}} = 1$ dB, L the path length and a' and b' the attenuation-form coefficients ($a' = a^{-1/b}$) corresponding to the frequency and polarization of the sublink. Results are grouped in three frequency bands, using the ITU relation (ITU, 2005) and the two Belgian relations obtained from the combined disdrometer observations. Symbols denote the median and the whiskers the interquartile range of the sublinks within each band, with the number of sublinks indicated at the bottom of the figure. The spread within a band is dominated by the distribution of path lengths. Note the logarithmic vertical axis and that no links are present between 45 and 65 GHz.

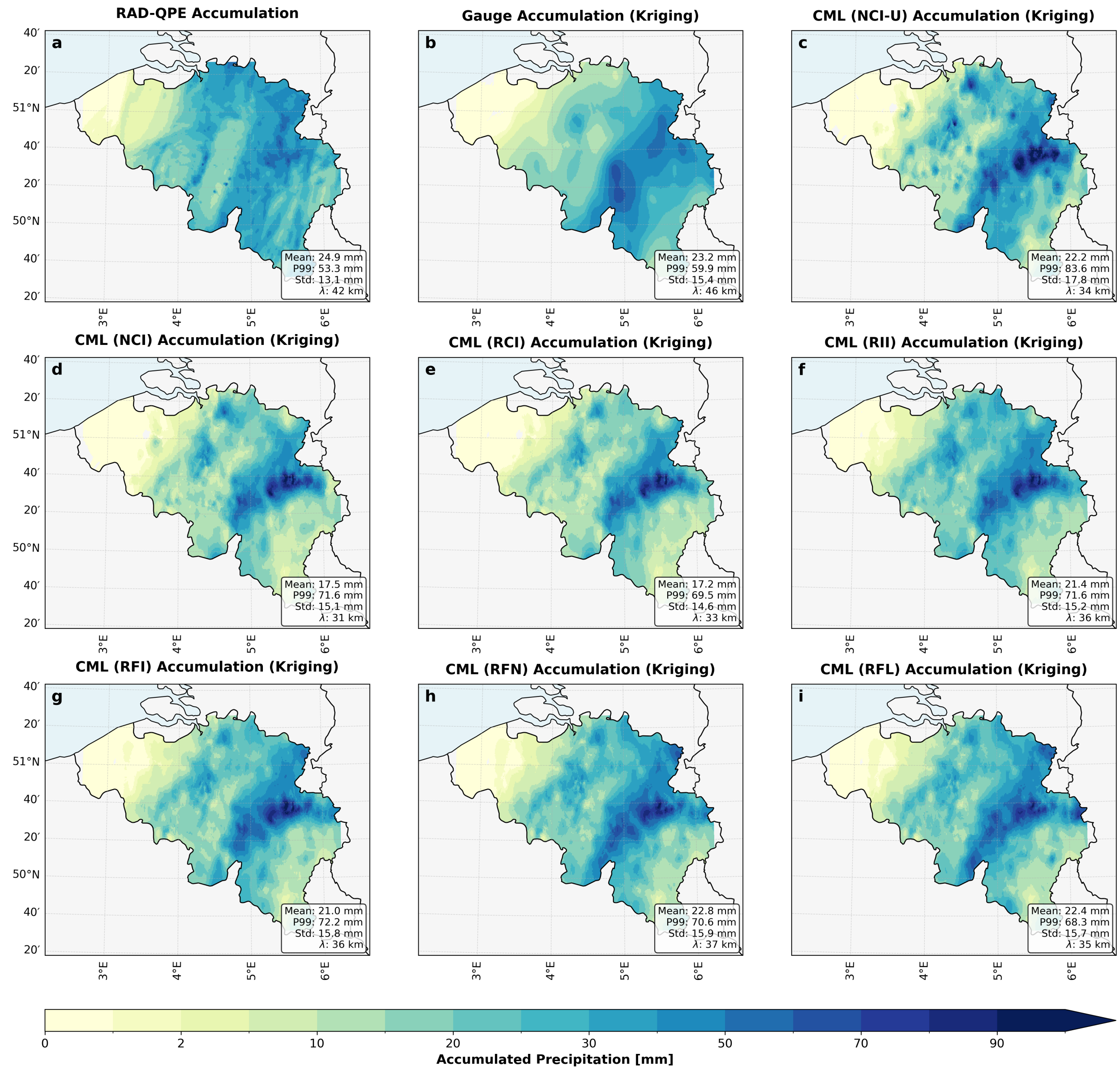

Figure 6: Accumulated rainfall during Case 1 from (a) RAD-QPE, (b) the rain gauges and (c–i) seven CML retrieval permutations, with the gauge and CML accumulations interpolated to the 1-km RAD-QPE grid using ordinary kriging (Section 2.3) and each CML treated as a point measurement at its midpoint. The permutations successively alter one processing step: outlier filtering (c, d), wet–dry classification (d, e), wet-antenna correction (e, f, g) and γ–R relation (g, h, i). The box in each panel lists the spatial mean, the 99th percentile (P99), the standard deviation (Std) and the autocorrelation length scale λ, computed as the e-folding radius of the radially averaged 2D autocorrelation. Corresponding maps for Cases 2 to 4 are provided in the supplementary material.

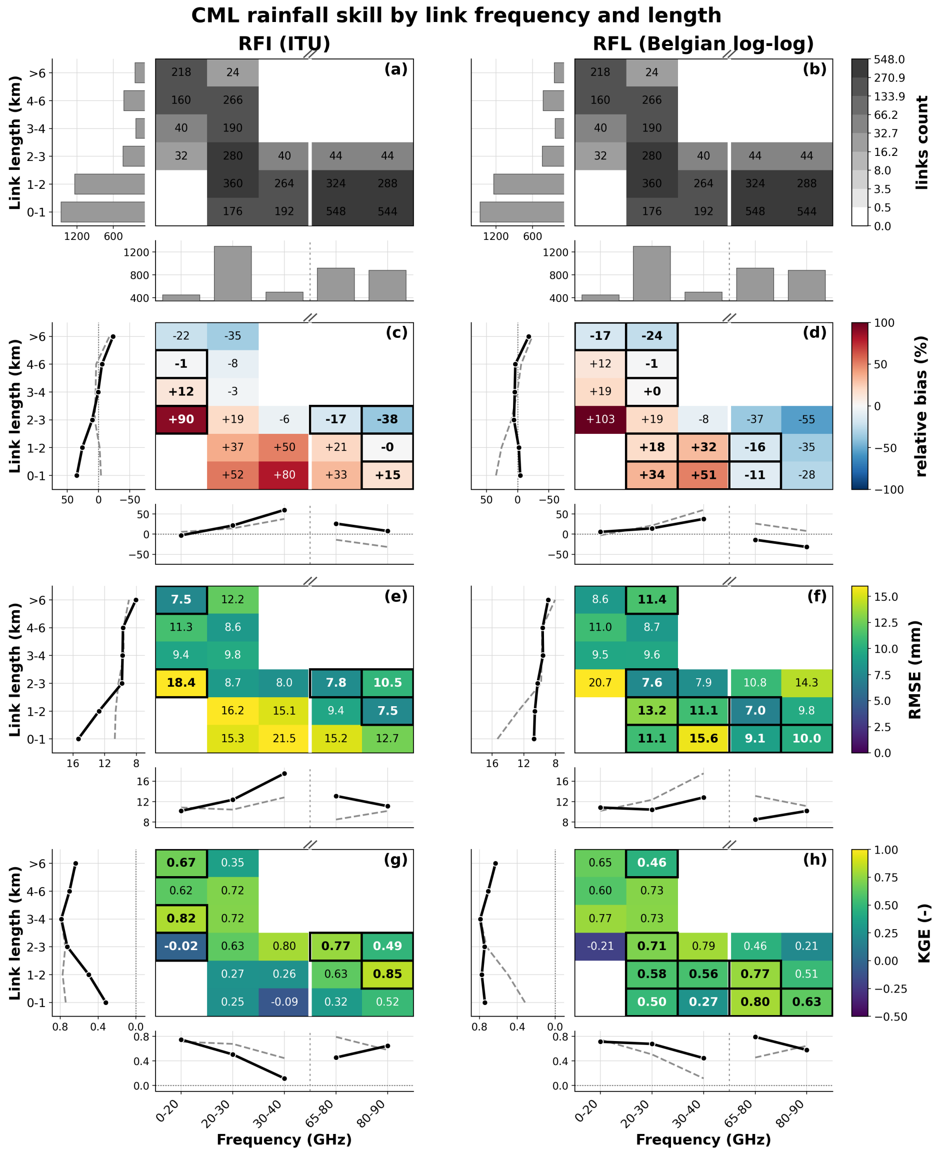

Figure 7: Per-link agreement with rain gauges as a function of link frequency (columns) and path length (rows), for the ITU relation (RFI, left column) and the Belgian log–log relation (RFL, right column). Panel rows show the number of gauge–CML pairs (a, b), relative bias (c, d), RMSE (e, f), and KGE (g, h), with a shared colour scale for RFI and RFL. Marginal profiles summarize each metric by pooling across frequency bins (left) or path-length bins (bottom), weighted by the number of pairs; KGE is recomputed from the pooled samples because it cannot be averaged across bins. In the metric marginals, the solid black line shows the experiment of the corresponding column and the dashed grey line the other experiment; count marginals are identical for both experiments and are shown as grey bars. The 45–65 GHz range contains no links and is omitted, and links ≥6 km are pooled into the top row. In the relative bias, RMSE, and KGE panels, the better-performing experiment in each bin is highlighted by a bold outline and value (relative bias: smaller absolute value). Statistics are computed for individual gauge–link pairs within a 2.5-km matching radius.

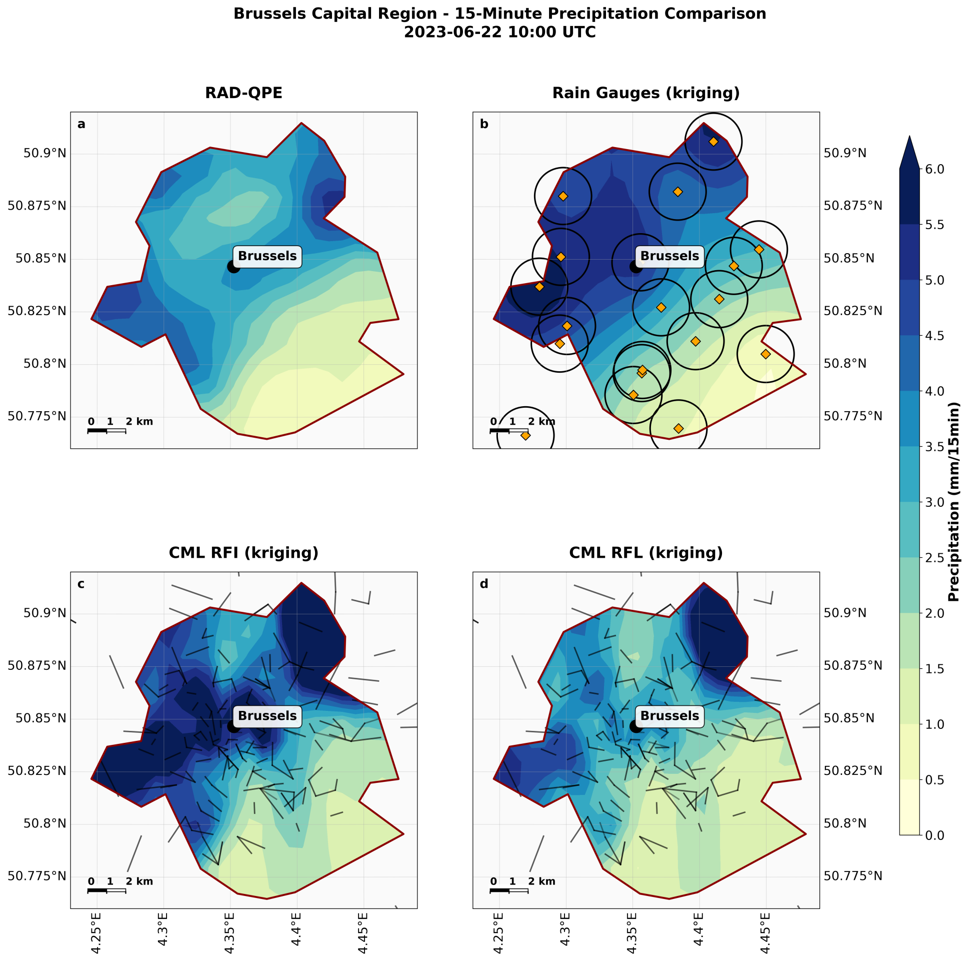

Figure 8: 15-min rainfall accumulation at 10:00 UTC on 22 June 2023 over the Brussels Capital Region (BCR), as obtained from (a) RAD-QPE, (b) the IBGE rain gauge network, (c) the RFI CML retrieval and (d) the RFL CML retrieval. Only data within the BCR are shown and the brown outline denotes its border. All data are regridded to the 1-km RAD-QPE grid using ordinary kriging. Gauge locations are indicated in panel b by orange diamonds, with a radius of 1 km drawn around them to focus on data that are not extrapolated too far from the gauges. Panels c and d also show the locations of all CMLs in the BCR.

2 Tables

Table 1: General statistics of case-accumulated precipitation across all 204 rain gauges shown in Figure 1 and for all cases. Shown are the case Duration, Mean Accumulations (Acc), 99th Percentile of the case-accumulations (P99) and the Standard Deviation of the accumulations (Std) across all stations.

Case	Duration	Acc (mm)	P99 (mm)	Std (mm)
Case 1	22 June 2023 (24 hours)	21.5	55.2	14.8
Case 2	8-9 July 2023 (48 hours)	3.0	15.7	3.4
Case 3	23-24 July 2023 (48 hours)	20.1	47.6	14.0
Case 4	28-29 July 2023 (48 hours)	10.5	46.3	10.3

Table 2: Naming convention of the CML rainfall retrieval permutations. Each permutation is identified by a three-letter acronym combining one option from each of the three processing steps (e.g., RIL = radar-based wet–dry classification, intensity-dependent wet-antenna correction, log–log Belgian $\gamma - \mathrm{R}$ relation). The suffix -U denotes retrievals without the outlier filtering of Section 3.2 (all other permutations are outlier-filtered). See text for details.

Position	Letter	Method	Reference
1 (Wet–Dry Classification)	N	Nearby links	Overeem et al. (2016a)
	R	Radar-based (RAD-QPE)	similar to Overeem et al. (2011)
2 (Wet-Antenna Correction)	C	Constant (2.3 dB)	Overeem et al. (2016a)
	I	Intensity-dependent	Pastorek et al. (2022)
	F	Frequency- and intensity-dependent	Leijnse et al. (2008)
3 ($\mathrm{R} - \gamma$ relation)	I	ITU recommendation	ITU (2005)
	N	Belgian disdrometers, nonlinear fit	Section ??
	L	Belgian disdrometers, log–log fit	Section ??
Suffix	-U	No outlier filtering (also retaining records with errored seconds)	Section ??

Table 3: Comparison of wet/dry detection skill based on contingency table statistics for the Nearby Link approach (N) and the RAD-QPE approach (R). Shown are the number of samples (n), Probability of Detection (POD), False Alarm Ratio (FAR), Critical Success Index (CSI), Percent Correct (PC), and Heidke Skill Score (HSS). Values are provided per case, and for all cases combined. Higher values indicate better performance for POD, CSI, PC, and HSS, whereas lower values indicate better performance for FAR.

Case	Method	n	POD	FAR	CSI	PC	HSS
All cases	N	48128	0.74	0.53	0.41	0.87	0.50
	R	48128	0.57	0.35	0.43	0.91	0.56
Case 1	N	8648	0.89	0.40	0.56	0.91	0.66
	R	8648	0.85	0.35	0.58	0.92	0.69
Case 2	N	13160	0.70	0.71	0.26	0.97	0.40
	R	13160	0.72	0.67	0.29	0.97	0.44
Case 3	N	13160	0.80	0.58	0.38	0.84	0.47
	R	13160	0.56	0.35	0.43	0.91	0.55
Case 4	N	13160	0.65	0.52	0.38	0.77	0.40
	R	13160	0.45	0.26	0.39	0.85	0.47

Table 4: Overview of the R–γ relation parameters, a (mm h^{-1}(km dB^{-1})$^{\mathrm{b}}$) and b (unitless) (Equation 3), for the inverted ITU (2005) relation, as fitted directly to the combined observations of the two disdrometers in Belgium using the log–log and the non-linear fit, and as documented in Overeem et al. (2016a) for The Netherlands, for frequencies of 10, 25 and 80 GHz and vertical polarization. The Belgian and Dutch coefficients are directly comparable to parameters a and b in Figure 2 of Overeem et al. (2016a). Relations fitted to the individual disdrometers are reported in the panels of Figure 4.

	ITU (inv.)		Belgium (log–log)		Belgium (non-lin.)		Netherlands (non-lin.)	
Frequency	a	b	a	b	a	b	a	b
10 GHz	39.98	0.82	60.17	0.87	39.52	0.75	37.71	0.75
25 GHz	7.21	1.05	8.07	0.90	8.28	0.93	8.11	0.95
80 GHz	0.80	1.42	1.03	1.08	0.94	1.18	1.00	1.34

Table 5: The five best-performing CML permutations per case and combined over all cases, ranked by KGE and compared with RAD-QPE, evaluated against the case-accumulated rain gauge observations (Section 3.6). For the CMLs all links with midpoints within 2.5 km, and for RAD-QPE all pixels within 2.5 km of the gauge are averaged. Only gauges with valid data for all products are included (n samples). The complete ranking of all 18 permutations is provided in the supplementary material (Table 10).

Product	n	KGE (–)	Bias (mm)	Rel. bias (%)	RMSE (mm)	R^2 (–)	r (–)
All cases							
RFL	387	0.85	0.2	1.7	7.3	0.71	0.85
RFN	387	0.83	1.0	7.6	7.4	0.69	0.86
RCN	387	0.83	-1.0	-7.6	7.3	0.70	0.85
NCL	387	0.82	-0.7	-5.4	7.9	0.65	0.84
RIL	387	0.81	1.6	12.0	7.6	0.68	0.85
RAD-QPE	387	0.65	4.0	29.1	8.6	0.59	0.83
Case 1							
NCN	102	0.78	-0.9	-4.1	9.1	0.55	0.80
NCL	102	0.77	-2.0	-9.6	9.0	0.56	0.79
RCN	102	0.76	-2.0	-9.7	9.2	0.54	0.79
RFL	102	0.76	0.5	2.4	9.5	0.51	0.77
NFL	102	0.75	1.7	8.2	9.5	0.50	0.78
RAD-QPE	102	0.66	4.5	21.2	9.8	0.47	0.77
Case 2							
RCN	103	0.69	0.4	12.2	2.6	0.53	0.75
NCN	103	0.68	0.3	7.6	2.7	0.48	0.72
RCL	103	0.68	0.2	5.2	2.5	0.56	0.75
NCL	103	0.65	0.0	0.3	2.7	0.48	0.70
NCI	103	0.63	0.5	16.3	3.2	0.29	0.68
RAD-QPE	103	-1.40	7.1	213.6	9.1	-4.68	0.76
Case 3							
RCN	99	0.77	-0.9	-4.3	9.5	0.55	0.78
RFN	99	0.76	2.1	9.8	9.5	0.55	0.78
RFL	99	0.75	0.6	3.0	9.1	0.59	0.78
RCL	99	0.72	-2.5	-11.5	9.6	0.54	0.77
RIL	99	0.72	2.7	12.4	9.9	0.51	0.76
RAD-QPE	99	0.69	2.7	12.8	9.1	0.59	0.79
Case 4							
RIN	83	0.57	-0.5	-5.5	5.0	0.57	0.77
RIL	83	0.55	-0.8	-9.6	5.1	0.56	0.77
RFN	83	0.52	-0.9	-11.0	5.3	0.53	0.75
RII	83	0.50	-0.6	-6.9	5.3	0.52	0.74
RFL	83	0.49	-1.3	-15.4	5.4	0.51	0.75
RAD-QPE	83	0.63	1.0	12.0	5.0	0.58	0.77

Table 6: Marginal effect of each processing choice, obtained by averaging the pooled evaluation metrics of Table S1 over all permutations sharing the respective option (N_{per} permutations each). Since the permutation set is a full 2×3×3 factorial, every option occurs equally often with all combinations of the other two factors, so that the averages are balanced. Options are ranked by mean KGE. Note that the values are mean scores across permutations rather than scores of a pooled product.

Option	N_{per}	KGE (−)	Bias (mm)	|Rel. bias| (%)	RMSE (mm)	R^2 (−)
Wet/dry classification						
Radar	9	0.785	0.68	9.6	7.89	0.653
Nearby link	9	0.598	2.31	18.1	10.29	0.401
Wet antenna attenuation						
Overeem 2016 (constant)	6	0.756	-0.39	5.9	8.51	0.589
Leijnse 2008 (freq./intensity)	6	0.704	1.74	12.7	8.96	0.542
Pastorek 2021 (intensity)	6	0.614	3.14	23.0	9.80	0.449
R-γ relation						
Belgium log-log	6	0.751	0.87	12.5	8.24	0.617
Belgium non-linear	6	0.712	1.62	14.4	8.78	0.562
ITU	6	0.611	2.00	14.7	10.25	0.402

Table 7: As Table 1, but for the IBGE network only, and including the average rain rates. Shown are the domain-average rain rate (mm h^{-1}), averaged over all 15-min intervals of the case, including the dry ones; the domain-average intensity (mm h^{-1}), averaged over the wet intervals only, that is, conditional on rainfall being recorded; the case-total accumulation (mm) and the case-accumulated 99th percentile (mm) and standard deviation (mm). The mean rate therefore reflects both the intensity and the temporal occurrence of rainfall, whereas the mean intensity characterises the rainfall when it occurs.

Case	Mean Rate (mm h^{-1})	Mean Intensity (mm h^{-1})	Mean Accumulation (mm)	P99 (mm)	Std (m
Case 1	1.08	5.3	26.0	33.7	7.9
Case 2	0.11	6.5	5.4	13.0	3.2
Case 3	0.79	6.0	37.9	42.4	3.3
Case 4	0.11	4.8	5.1	7.7	1.6
Overall	0.44	5.7	18.6	42.3	14.7

Table 8: The five best-performing CML permutations per case and combined over all cases, ranked by KGE and compared with RAD-QPE, evaluated against the 15-minute rainfall observations of the IBGE network in the BCR. For each gauge, the CML retrievals are averaged over all links with midpoints within 1 km, and RAD-QPE is taken as the average of the grid points within the same radius. n_{sam} denotes the number of 15-minute samples pooled over all gauges. The complete ranking of all 18 permutations is provided in the supplementary material (Table 11).

Product	n_{sam}	KGE (–)	Bias (mm/15 min)	Rel. bias (%)	RMSE (mm/15 min)	R^2 (–)	r (–)
All cases							
RFL	7073	0.83	0.005	4.2	0.283	0.68	0.84
RCL	7073	0.81	-0.007	-5.5	0.295	0.65	0.82
RIL	7073	0.80	0.017	13.8	0.269	0.71	0.85
RCN	7073	0.76	0.007	6.1	0.329	0.57	0.82
RFN	7073	0.76	0.017	14.1	0.308	0.62	0.83
RAD-QPE	7073	0.66	0.024	19.6	0.381	0.42	0.74
Case 1							
NCN	1047	0.88	0.011	3.5	0.372	0.80	0.90
RCN	1047	0.86	-0.024	-7.4	0.363	0.81	0.90
RFN	1047	0.84	0.032	10.1	0.384	0.79	0.89
NCL	1047	0.79	-0.015	-4.7	0.379	0.79	0.89
RFL	1047	0.79	0.012	3.7	0.394	0.78	0.88
RAD-QPE	1047	0.72	0.064	20.1	0.372	0.80	0.90
Case 2							
RCL	2208	0.62	0.003	13.2	0.193	0.28	0.65
RFL	2208	0.62	0.004	17.6	0.183	0.36	0.67
NCL	2208	0.62	0.004	16.1	0.193	0.29	0.65
NFL	2208	0.61	0.005	21.1	0.183	0.36	0.67
RIL	2208	0.56	0.007	30.4	0.177	0.40	0.69
RAD-QPE	2208	-2.10	0.059	249.0	0.501	-3.81	0.76
Case 3							
RIL	2024	0.84	0.014	7.0	0.331	0.72	0.86
RFL	2024	0.83	0.005	2.5	0.362	0.66	0.84
RCL	2024	0.80	-0.004	-2.1	0.391	0.60	0.82
RIN	2024	0.72	0.038	18.3	0.374	0.64	0.86
RFN	2024	0.70	0.030	14.4	0.413	0.56	0.83
RAD-QPE	2024	0.69	-0.026	-12.4	0.338	0.70	0.84
Case 4							
RIL	1794	0.53	0.001	4.5	0.165	0.06	0.70
RFL	1794	0.38	0.002	8.0	0.188	-0.22	0.70
RIN	1794	0.36	0.004	15.2	0.187	-0.22	0.70
RCL	1794	0.27	0.003	10.2	0.205	-0.46	0.69
RFN	1794	0.16	0.005	20.6	0.218	-0.65	0.69
RAD-QPE	1794	0.10	0.012	44.4	0.232	-0.86	0.57

3 Review Tables and Figures

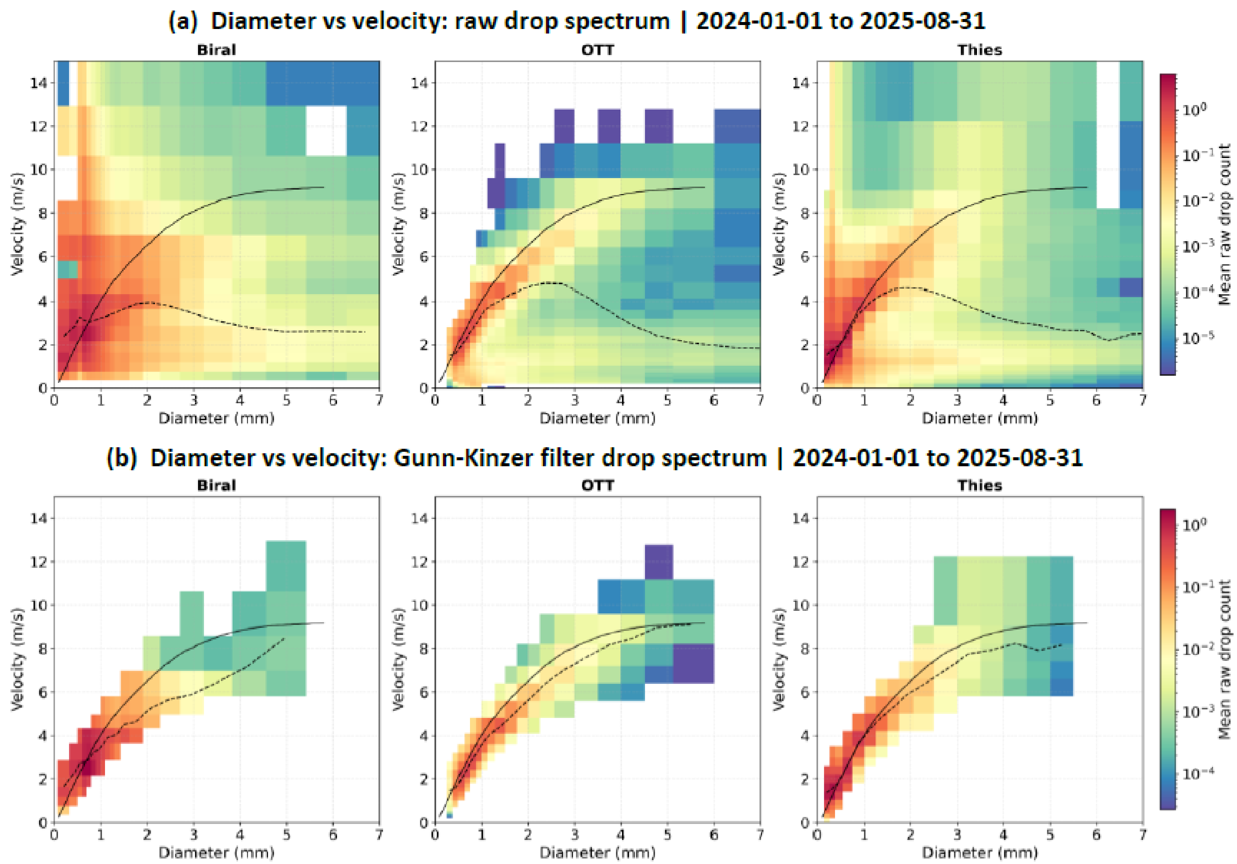

Figure 9: Raw (a) and filterd (b) drop spectra of the three disdrometers in Belgium (left: Biral in Uccle; middle: OTT Parsivel in Melle; right: Thies Climate in Sart Tilman). The population of low-velocity/ large diameter particles in all disdrometers are snowflakes, which are filtered out. The Biral disdrometer has a very large number of particles with small diameters and high velocitity as well, and no clear rain signature like the other two disdrometers.

Table 9: Sensitivity of the evaluation to the gauge–CML pairing rule. Each row repeats the full evaluation of all 18 processing permutations for one pairing rule: the radius-mean rules average all links whose midpoint lies within the stated radius of the gauge, while the last row pairs each gauge with its single nearest link and discards gauges whose nearest link lies further than 5 km. The 2.5 km row is the configuration used in the manuscript. The left-hand block scores each pairing rule on its own set of matched gauges, whose size n (the number of case-combined gauge samples over the four cases) necessarily grows with the radius; the right-hand block repeats the exercise on the $n_{\text{fix}} = 126$ samples that all pairing rules have in common, so that the estimator can be compared at constant sample. *Best permutation* is the three-letter code of the permutation with the highest KGE under that pairing, and *KGE*, *Rel. bias* and *RMSE* characterise that best permutation. The two radar columns give the corresponding RAD-QPE benchmark on the same gauges, sampled in two ways: *RAD-QPE (point)* takes the single radar grid point nearest to the gauge and is therefore independent of the CML pairing, so that any variation down that column reflects only the changing station set; *RAD-QPE (area)* averages the radar over the same radius as the CMLs and therefore shares their spatial support. On the common sample the point radar is by construction identical for every row (KGE = 0.73) and is omitted from the right-hand block. The area-averaged radar is not meaningful for the nearest-link rule, where it would average radar over 5 km against a single link, and that value should be disregarded.

	Own matched gauges							Common gauges ($n_{\text{fix}} = 126$)		
		Best permutation				RAD-QPE		Best perm.		RAD-QPE
Pairing rule	n	Code	KGE (–)	Rel. bias (%)	RMSE (mm)	point (–)	area (–)	Code	KGE (–)	area (–)
Radius mean, 1 km	126	RCL	0.82	−10.8	8.25	0.73	0.73	RCL	0.82	0.73
Radius mean, 1.5 km	224	RFL	0.87	−1.5	7.42	0.72	0.72	RCN	0.84	0.73
Radius mean, 2 km	326	RFL	0.85	−0.4	7.30	0.68	0.68	RCN	0.89	0.73
Radius mean, 2.5 km	387	RFL	0.85	1.7	7.29	0.65	0.65	RCN	0.91	0.73
Radius mean, 3 km	445	RFL	0.82	2.0	7.94	0.66	0.66	RCN	0.91	0.73
Radius mean, 5 km	638	RFN	0.83	7.2	7.80	0.67	0.66	RCN	0.90	0.72
Radius mean, 10 km	773	RFI	0.83	6.4	7.83	0.67	0.65	NCL	0.91	0.70
Nearest link, ≤5 km	664	RFL	0.73	3.9	10.53	0.68	0.67	RCL	0.75	0.72

4 Supplementary Material

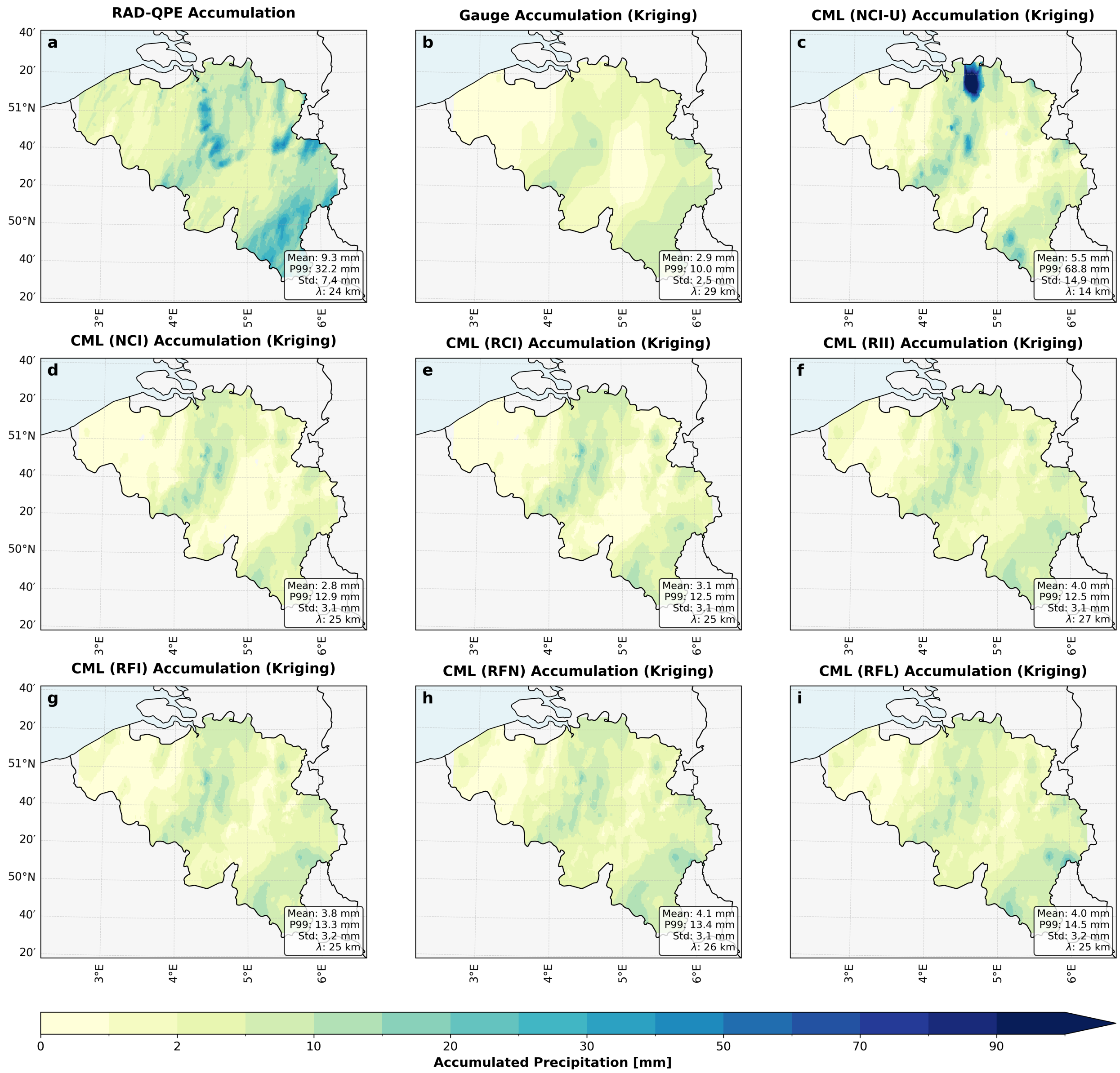

Figure 10: As Figure 6, but for case 2.

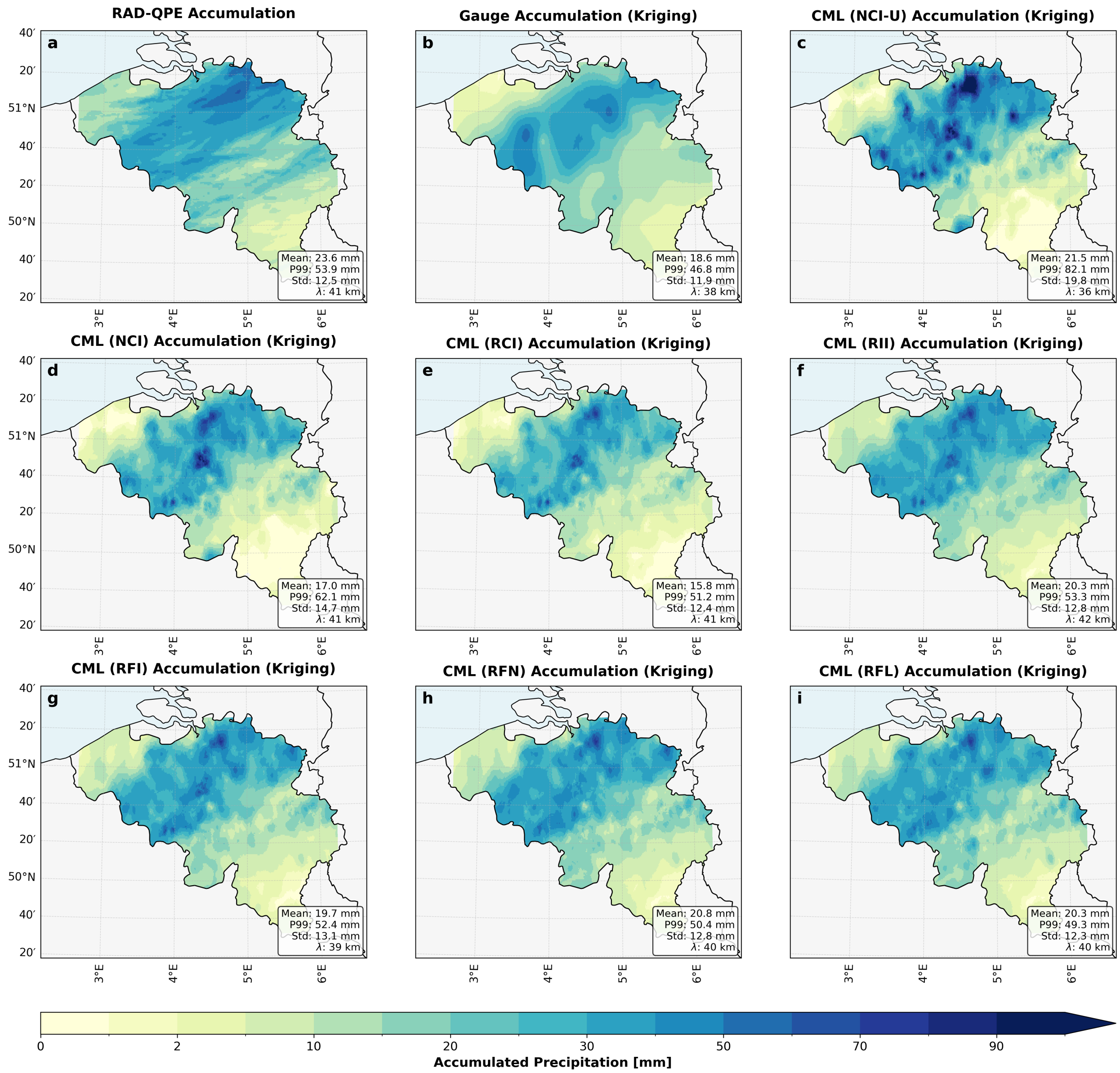

Figure 11: As Figure 6, but for case 3.

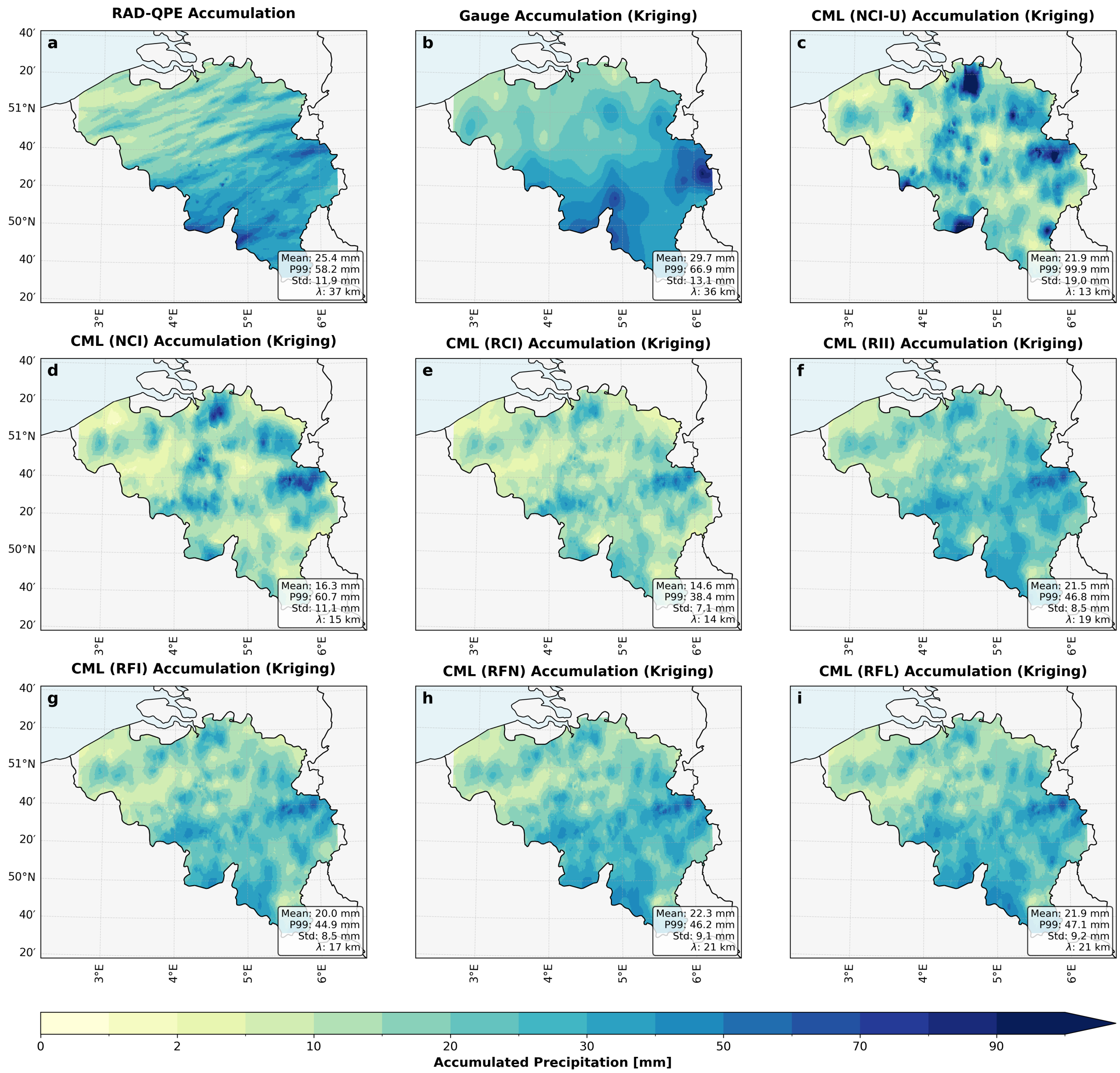

Figure 12: As Figure 6, but for case 4.

Table 10: As Table 5, but for the complete ranking of all 18 permutations.

Product	n	KGE (–)	Bias (mm)	Rel. bias (%)	RMSE (mm)	R^2 (–)	r (–)
All cases							
RFL	387	0.85	0.2	1.7	7.3	0.71	0.85
RFN	387	0.83	1.0	7.6	7.4	0.69	0.86
RCN	387	0.83	-1.0	-7.6	7.3	0.70	0.85
NCL	387	0.82	-0.7	-5.4	7.9	0.65	0.84
RIL	387	0.81	1.6	12.0	7.6	0.68	0.85
RCL	387	0.77	-1.8	-13.1	7.4	0.70	0.85
NCN	387	0.77	0.2	1.1	8.6	0.59	0.83
RCI	387	0.77	0.0	0.1	8.7	0.58	0.83
RIN	387	0.76	2.3	16.8	8.0	0.65	0.85
RFI	387	0.76	1.4	10.0	8.4	0.61	0.85
NFL	387	0.70	2.1	15.1	9.0	0.55	0.84
RII	387	0.70	2.4	17.3	8.9	0.56	0.85
NFN	387	0.60	2.8	20.5	10.0	0.44	0.84
NCI	387	0.57	1.1	7.8	11.1	0.31	0.80
NIL	387	0.56	3.8	27.7	10.3	0.42	0.84
NFI	387	0.49	2.9	21.4	11.6	0.25	0.82
NIN	387	0.48	4.5	32.7	11.3	0.30	0.84
NII	387	0.38	4.3	31.5	12.8	0.09	0.81
RAD-QPE	387	0.65	4.0	29.1	8.6	0.59	0.83
Case 1							
NCN	102	0.78	-0.9	-4.1	9.1	0.55	0.80
NCL	102	0.77	-2.0	-9.6	9.0	0.56	0.79
RCN	102	0.76	-2.0	-9.7	9.2	0.54	0.79
RFL	102	0.76	0.5	2.4	9.5	0.51	0.77
NFL	102	0.75	1.7	8.2	9.5	0.50	0.78
RCL	102	0.75	-2.9	-13.7	9.2	0.54	0.79
RFN	102	0.74	1.6	7.5	9.6	0.50	0.79
RIL	102	0.73	3.1	14.8	9.8	0.47	0.78
NFN	102	0.71	2.8	13.1	10.0	0.45	0.79
RFI	102	0.70	1.1	5.2	10.1	0.44	0.79
RCI	102	0.70	-1.7	-7.8	10.4	0.41	0.77
RIN	102	0.68	3.8	18.3	10.4	0.40	0.78
NCI	102	0.68	-0.4	-1.8	10.6	0.39	0.77
NIL	102	0.67	4.4	21.0	10.6	0.38	0.77
NFI	102	0.65	2.4	11.4	10.9	0.35	0.78
RII	102	0.63	3.1	14.5	11.5	0.27	0.75
NIN	102	0.62	5.3	25.2	11.4	0.29	0.78
NII	102	0.55	4.7	22.4	12.7	0.12	0.74
RAD-QPE	102	0.66	4.5	21.2	9.8	0.47	0.77
Case 2							
RCN	103	0.69	0.4	12.2	2.6	0.53	0.75

NCN	103	0.68	0.3	7.6	2.7	0.48	0.72
RCL	103	0.68	0.2	5.2	2.5	0.56	0.75
NCL	103	0.65	0.0	0.3	2.7	0.48	0.70
NCI	103	0.63	0.5	16.3	3.2	0.29	0.68
RCI	103	0.62	0.7	22.0	3.2	0.30	0.70
RFL	103	0.61	0.8	23.5	2.6	0.52	0.75
NFL	103	0.60	0.8	22.7	3.0	0.39	0.69
NFN	103	0.59	0.9	27.8	3.0	0.37	0.70
RFN	103	0.58	1.0	31.2	2.8	0.44	0.74
NFI	103	0.57	1.0	29.8	3.2	0.27	0.69
RFI	103	0.56	1.1	33.8	3.1	0.33	0.72
RIL	103	0.53	1.2	34.9	2.8	0.47	0.76
NIL	103	0.52	1.2	35.7	3.1	0.31	0.69
RIN	103	0.51	1.3	40.4	2.9	0.41	0.74
RII	103	0.49	1.4	41.6	3.2	0.27	0.71
NII	103	0.48	1.3	40.0	3.4	0.19	0.68
NIN	103	0.48	1.4	41.1	3.3	0.25	0.68
RAD-QPE	103	-1.40	7.1	213.6	9.1	-4.68	0.76
Case 3							
RCN	99	0.77	-0.9	-4.3	9.5	0.55	0.78
RFN	99	0.76	2.1	9.8	9.5	0.55	0.78
RFL	99	0.75	0.6	3.0	9.1	0.59	0.78
RCL	99	0.72	-2.5	-11.5	9.6	0.54	0.77
RIL	99	0.72	2.7	12.4	9.9	0.51	0.76
RIN	99	0.71	4.0	18.6	10.4	0.46	0.77
NCL	99	0.68	1.3	5.9	10.8	0.42	0.79
RFI	99	0.61	3.8	17.6	11.6	0.33	0.80
RII	99	0.59	5.1	23.8	11.7	0.32	0.81
RCI	99	0.56	2.1	9.8	12.0	0.28	0.80
NCN	99	0.54	3.1	14.3	12.5	0.22	0.78
NFL	99	0.47	6.4	30.1	13.4	0.11	0.81
NFN	99	0.33	7.9	36.9	15.8	-0.23	0.78
NIL	99	0.33	9.3	43.6	15.9	-0.25	0.79
NIN	99	0.20	10.8	50.3	17.8	-0.57	0.79
NCI	99	0.15	5.7	26.6	17.8	-0.57	0.77
NFI	99	0.09	8.8	41.3	18.9	-0.78	0.78
NII	99	-0.01	11.1	52.1	20.5	-1.09	0.79
RAD-QPE	99	0.69	2.7	12.8	9.1	0.59	0.79
Case 4							
RIN	83	0.57	-0.5	-5.5	5.0	0.57	0.77
RIL	83	0.55	-0.8	-9.6	5.1	0.56	0.77
RFN	83	0.52	-0.9	-11.0	5.3	0.53	0.75
RII	83	0.50	-0.6	-6.9	5.3	0.52	0.74
RFL	83	0.49	-1.3	-15.4	5.4	0.51	0.75
RFI	83	0.49	-0.8	-10.3	5.5	0.50	0.73
RCN	83	0.44	-1.7	-21.3	5.6	0.47	0.75
NIL	83	0.44	-0.4	-4.9	6.4	0.31	0.56

NFN	83	0.44	-0.9	-11.3	6.3	0.32	0.58
RCI	83	0.43	-1.3	-16.2	5.9	0.42	0.68
NFL	83	0.43	-1.1	-13.7	6.3	0.33	0.59
RCL	83	0.41	-2.1	-25.8	5.7	0.45	0.76
NIN	83	0.41	-0.3	-3.1	6.6	0.27	0.53
NFI	83	0.37	-1.1	-13.5	6.8	0.22	0.51
NII	83	0.35	-0.7	-8.3	6.9	0.18	0.47
NCL	83	0.33	-2.5	-30.4	6.6	0.26	0.61
NCN	83	0.32	-2.2	-26.9	6.8	0.22	0.55
NCI	83	0.27	-2.0	-24.5	7.3	0.11	0.44
RAD-QPE	83	0.63	1.0	12.0	5.0	0.58	0.77

Table 11: As Table 8, but for the complete ranking of all 18 permutations.

Product	n	KGE (–)	Bias (mm/15 min)	Rel. bias (%)	RMSE (mm/15 min)	R^2 (–)	r (–)
All cases							
RCL	8133	0.77	-0.003	-2.7	0.315	0.57	0.77
RFL	8133	0.77	0.008	6.5	0.311	0.58	0.78
RIL	8133	0.73	0.019	16.1	0.306	0.59	0.79
RCN	8133	0.73	0.010	8.9	0.346	0.48	0.77
RFN	8133	0.71	0.020	16.8	0.336	0.51	0.78
RIN	8133	0.65	0.031	26.4	0.329	0.53	0.79
NCL	8133	0.64	0.027	23.3	0.360	0.44	0.75
NFL	8133	0.50	0.049	42.3	0.357	0.45	0.76
NCN	8133	0.48	0.043	36.8	0.406	0.29	0.75
NIL	8133	0.36	0.068	58.2	0.356	0.45	0.77
RFI	8133	0.36	0.047	40.7	0.451	0.12	0.76
NFN	8133	0.35	0.063	54.2	0.398	0.32	0.76
RII	8133	0.31	0.059	50.6	0.434	0.19	0.78
RCI	8133	0.27	0.048	40.8	0.501	-0.08	0.75
NIN	8133	0.23	0.081	69.7	0.389	0.34	0.77
NFI	8133	-0.01	0.090	77.1	0.528	-0.21	0.75
NCI	8133	-0.02	0.080	69.0	0.575	-0.43	0.73
NII	8133	-0.09	0.106	90.7	0.500	-0.08	0.76
RAD-QPE	8133	0.68	0.023	19.5	0.349	0.47	0.77
Case 1							
RCN	1141	0.84	0.010	3.7	0.401	0.72	0.85
NCL	1141	0.79	0.018	6.2	0.402	0.72	0.85
NCN	1141	0.78	0.044	15.4	0.417	0.70	0.85
RCL	1141	0.78	-0.011	-3.8	0.392	0.73	0.85
RFL	1141	0.74	0.045	15.9	0.402	0.72	0.85
RFN	1141	0.72	0.066	23.3	0.410	0.71	0.85
NFL	1141	0.68	0.070	24.8	0.412	0.70	0.84
NFN	1141	0.64	0.092	32.5	0.420	0.69	0.85
RCI	1141	0.62	0.059	20.9	0.518	0.53	0.85
RIL	1141	0.60	0.098	34.5	0.432	0.67	0.83
RFI	1141	0.59	0.094	33.2	0.475	0.60	0.86
RIN	1141	0.55	0.120	42.2	0.437	0.67	0.84
NCI	1141	0.51	0.101	35.5	0.545	0.48	0.84
NIL	1141	0.49	0.132	46.4	0.461	0.63	0.82
NFI	1141	0.45	0.136	47.8	0.510	0.55	0.85
NIN	1141	0.42	0.157	55.2	0.474	0.61	0.83
RII	1141	0.39	0.157	55.2	0.495	0.57	0.86
NII	1141	0.22	0.204	72.0	0.548	0.47	0.84
RAD-QPE	1141	0.65	0.087	30.6	0.392	0.73	0.86
Case 2							
NCN	2392	0.58	0.003	9.9	0.236	0.27	0.61
RCN	2392	0.58	0.003	8.8	0.236	0.27	0.60

RFN	2392	0.58	0.003	11.9	0.229	0.31	0.62
NFN	2392	0.57	0.004	14.9	0.231	0.30	0.61
NCL	2392	0.56	-0.001	-1.8	0.224	0.34	0.61
NFL	2392	0.56	0.001	4.8	0.221	0.36	0.62
RIL	2392	0.55	0.002	7.3	0.217	0.38	0.63
RCL	2392	0.55	-0.001	-4.7	0.223	0.35	0.61
RIN	2392	0.55	0.006	20.9	0.229	0.31	0.62
RFL	2392	0.54	-0.000	-0.1	0.221	0.36	0.61
NIL	2392	0.53	0.004	14.5	0.222	0.35	0.61
NIN	2392	0.53	0.007	25.0	0.230	0.31	0.62
NFI	2392	0.39	0.012	40.7	0.281	-0.04	0.58
RFI	2392	0.38	0.012	40.7	0.283	-0.05	0.58
RII	2392	0.35	0.014	47.5	0.275	0.00	0.59
NII	2392	0.32	0.015	51.1	0.275	0.00	0.59
NCI	2392	0.32	0.013	43.6	0.303	-0.20	0.57
RCI	2392	0.29	0.014	46.9	0.307	-0.24	0.57
RAD-QPE	2392	-1.04	0.046	158.7	0.415	-1.27	0.87
Case 3							
RIL	2392	0.78	0.014	6.8	0.391	0.59	0.79
RFL	2392	0.77	0.003	1.5	0.412	0.55	0.77
RCL	2392	0.76	-0.005	-2.5	0.424	0.52	0.76
RFN	2392	0.69	0.028	13.5	0.457	0.44	0.77
RIN	2392	0.69	0.038	18.4	0.432	0.50	0.79
RCN	2392	0.67	0.023	11.4	0.479	0.39	0.76
NCL	2392	0.50	0.072	35.3	0.509	0.31	0.75
NFL	2392	0.35	0.113	55.0	0.504	0.32	0.77
NCN	2392	0.28	0.106	51.7	0.594	0.06	0.75
NIL	2392	0.27	0.137	66.9	0.486	0.37	0.78
RII	2392	0.24	0.100	49.0	0.617	-0.02	0.77
RFI	2392	0.22	0.093	45.2	0.654	-0.14	0.75
NFN	2392	0.15	0.143	69.9	0.583	0.09	0.76
NIN	2392	0.09	0.165	80.5	0.551	0.19	0.77
RCI	2392	0.08	0.105	51.1	0.731	-0.43	0.74
NII	2392	-0.30	0.215	105.1	0.747	-0.49	0.76
NFI	2392	-0.31	0.201	98.0	0.806	-0.74	0.74
NCI	2392	-0.35	0.187	91.5	0.878	-1.06	0.73
RAD-QPE	2392	0.69	-0.024	-11.5	0.342	0.69	0.83
Case 4							
RIL	2208	0.52	0.001	2.8	0.180	-0.08	0.57
RFL	2208	0.47	0.001	3.6	0.192	-0.23	0.56
RCL	2208	0.45	0.001	2.5	0.195	-0.27	0.57
RIN	2208	0.41	0.004	14.5	0.201	-0.34	0.56
RFN	2208	0.34	0.004	15.0	0.213	-0.52	0.56
RCN	2208	0.27	0.005	17.1	0.224	-0.67	0.57
NCL	2208	0.07	0.013	46.2	0.242	-0.94	0.55
RII	2208	-0.05	0.012	42.9	0.267	-1.37	0.55
NFL	2208	-0.06	0.021	75.7	0.230	-0.77	0.56

RFI	2208	-0.16	0.013	44.5	0.286	-1.71	0.55
NCN	2208	-0.17	0.018	61.6	0.273	-1.49	0.55
NIL	2208	-0.19	0.028	99.5	0.216	-0.56	0.56
NFN	2208	-0.25	0.025	88.3	0.256	-1.18	0.55
NIN	2208	-0.34	0.031	110.1	0.236	-0.86	0.55
RCI	2208	-0.42	0.016	56.5	0.323	-2.47	0.56
NII	2208	-0.59	0.034	118.7	0.286	-1.72	0.54
NFI	2208	-0.65	0.030	105.9	0.321	-2.43	0.54
NCI	2208	-0.77	0.027	94.1	0.359	-3.28	0.54
RAD-QPE	2208	-0.06	0.014	48.8	0.237	-0.88	0.72

References

Ghiggi, G., Candolfi, K., Billaux-Roux, A.-C., Longchamps, R., Pham-Ba, S., Weil, C., and Berne, A.: disdrodb: an open-source Python package for standardized processing, sharing, and analysis of disdrometer data, EGUsphere, 2026, 1–71, https://doi.org/10.5194/egusphere-2026-1886, 2026.

Gupta, H. V., Kling, H., Yilmaz, K. K., and Martinez, G. F.: Decomposition of the mean squared error and NSE performance criteria: Implications for improving hydrological modelling, Journal of Hydrology, 377, 80–91, https://doi.org/https://doi.org/10.1016/j.jhydrol.2009.08.003, 2009.

ITU: Recommendation ITU-R P.838-3, Specific attenuation model for rain for use in prediction methods, Tech. rep., International Telecommunication Union, `https://www.itu.int/dms`$_{p}ubrec/itu-r/rec/p/R-REC-P.838-3-200503-I!!PDF-E.pdf$, 2005.

Journée, M., Goudenhoofdt, E., Vannitsem, S., and Delobbe, L.: Quantitative rainfall analysis of the 2021 mid-July flood event in Belgium, Hydrology and Earth System Sciences, 27, 3169–3189, https://doi.org/10.5194/hess-27-3169-2023, 2023.

Leijnse, H., Uijlenhoet, R., and Stricker, J.: Microwave link rainfall estimation: Effects of link length and frequency, temporal sampling, power resolution, and wet antenna attenuation, Advances in Water Resources, 31, 1481–1493, https://doi.org/https://doi.org/10.1016/j.advwatres.2008.03.004, 2008.

Overeem, A., Leijnse, H., and Uijlenhoet, R.: Measuring urban rainfall using microwave links from commercial cellular communication networks, Water Resources Research, 47, https://doi.org/https://doi.org/10.1029/2010WR010350, 2011.

Overeem, A., Leijnse, H., and Uijlenhoet, R.: Retrieval algorithm for rainfall mapping from microwave links in a cellular communication network, Atmospheric Measurement Techniques, 9, 2425–2444, https://doi.org/10.5194/amt-9-2425-2016, 2016a.

Overeem, A., Leijnse, H., and Uijlenhoet, R.: Two and a half years of country-wide rainfall maps using radio links from commercial cellular telecommunication networks, Water Resources Research, 52, 8039–8065, https://doi.org/https://doi.org/10.1002/2016WR019412, 2016b.

Pastorek, J., Fencl, M., Rieckermann, J., and Bareš, V.: Precipitation Estimates From Commercial Microwave Links: Practical Approaches to Wet-Antenna Correction, IEEE Transactions on Geoscience and Remote Sensing, 60, 1–9, https://doi.org/10.1109/TGRS.2021.3110004, 2022.

Pu, K., Liu, X., and He, H.: Wet Antenna Attenuation Model of E-Band Microwave Links Based on the LSTM Algorithm, IEEE Antennas and Wireless Propagation Letters, 19, 1586–1590, https://doi.org/10.1109/LAWP.2020.3011463, 2020.

Roversi, G., Alberoni, P. P., Fornasiero, A., and Porcù, F.: Commercial microwave links as a tool for operational rainfall monitoring in Northern Italy, Atmospheric Measurement Techniques, 13, 5779–5797, https://doi.org/10.5194/amt-13-5779-2020, 2020.

Schleiss, M. and Berne, A.: Identification of Dry and Rainy Periods Using Telecommunication Microwave Links, IEEE Geoscience and Remote Sensing Letters, 7, 611–615, https://doi.org/10.1109/LGRS.2010.2043052, 2010.

Schleiss, M., Rieckermann, J., and Berne, A.: Quantification and Modeling of Wet-Antenna Attenuation for Commercial Microwave Links, IEEE Geoscience and Remote Sensing Letters, 10, 1195–1199, https://doi.org/10.1109/LGRS.2012.2236074, 2013.

Valtr, P., Fencl, M., and Bareš, V.: Excess Attenuation Caused by Antenna Wetting of Terrestrial Microwave Links at 32 GHz, IEEE Antennas and Wireless Propagation Letters, 18, 1636–1640, https://doi.org/10.1109/LAWP.2019.2925455, 2019.

van de Beek, C., Leijnse, H., Torfs, P., and Uijlenhoet, R.: Seasonal semi-variance of Dutch rainfall at hourly to daily scales, Advances in Water Resources, 45, 76–85, https://doi.org/https://doi.org/10.1016/j.advwatres.2012.03.023, space-Time Precipitation from Urban Scale to Global Change, 2012.